Title: Height does not impair the hydraulic system of the tallest tropical Dipterocarp trees

Authors: Paulo Bittencourt[1,2]*†, Arne Scheire[2]†, Palasiah Jotan[3]†, Jehova Lourenço-Junior[4], Lindsay F Banin[5], Mohd. Aminur Faiz bin Suis[6,7], David FRP Burslem[8], Bradley Christoffersen[9], David Coomes[10], Peter Groenendijk[11], Steven Jansen[12], Tommaso Jucker[13], Radim Matula[3], Maurizio Mencuccini[14,15], Rafael Oliveira[11], Roman Plichta[16], Reuben Nilus[6], Rolando Robert[6], Martin Svátek[16], Lucy Rowland[2]

Affiliations:

[1] School of Earth and Environmental Sciences, Cardiff University; Cardiff, CF10 3AT, UK.

[2] Faculty of Environment, Science and Economy, University of Exeter, Exeter; EX4 4QJ, UK.

[3] Department of Forest Ecology, Faculty of Forestry and Wood Sciences, Czech University of Life Sciences Prague; Prague, 165 00, Czech Republic.

[4] Royal Botanic Gardens, Kew; Richmond, TW9 3AE, UK.

[5] UK Centre for Ecology & Hydrology; Penicuik, Midlothian, EH26 0QB, UK.

[6] Sabah Forestry Department, Forest Research Centre; Sandakan, 90715, Malaysia.

[7] Research Management Centre, Universiti Malaysia Sabah; Kota Kinabalu, 88400, Malaysia.

[8] Interdisciplinary Institute and School of Biological Sciences, University of Aberdeen; Aberdeen, AB24 3FX, UK.

[9] School of Integrative Biological and Chemical Sciences, University of Texas Rio Grande Valley; Edinburg, 78539, USA.

[10] Conservation Research Institute and Department of Plant Sciences, University of Cambridge; Cambridge, CB2 1TN, UK.

[11] Department of Plant Biology, Institute of Biology, P.O. Box: 6109, University of Campinas (UNICAMP), 13083-970, Campinas, SP, Brazil .

[12] Institute of Botany, Ulm University; Ulm, 89081, Germany.

[13] School of Biological Sciences, University of Bristol; Bristol, BS8 1TH, UK.

[14] Centre de Recerca i Aplicacions Forestals (CREAF); Barcelona, 08193, Spain.

[15] Institución Catalana de Investigación y Estudios Avanzados (ICREA); Barcelona, 08010, Spain.

[16] Department of Forest Botany, Dendrology and Geobiocoenology, Faculty of Forestry and Wood Technology, Mendel University in Brno; Brno, 613 00, Czech Republic.

*Corresponding author. Email: BittencourtP@cardiff.ac.uk.

Abstract: Half the above-ground biomass in forests is stored in a disproportionately small number of very tall trees. These giants are predicted to be more vulnerable to drought-induced damage because height impairs their hydraulic system. We evaluated whether the hydraulic system of world's tallest tropical tree species – South-East Asian dipterocarps – are negatively impacted by their height. The more negative xylem pressures caused by tree height were fully compensated for through adjusting vessel anatomy and leaf hydraulic traits, and they suffered no height-related loss in growth during a severe drought. Therefore, height does not make the hydraulic systems of the world's tallest tropical tree species more vulnerable to drought and the growth rates of these trees are not more negatively impacted by drought than their smaller counterparts.

Main Text:

The tallest 1% of trees store more than half of aboveground carbon (*1–3*) and are predicted to face higher drought mortality risk, with consequences for global carbon stocks (*4–7*). With increasing height, gravity lowers leaf water potential and longer water transport path lengths raise hydraulic resistances (*8*, *9*). Theory and empirical data suggest that as a tree grows taller tip-to-base widening of water-conducting vessels can buffer these effects and maintain water supply to the leaves (*10–17*). Wider vessels lower hydraulic resistance, so continual widening with height growth can keep pace with the drops in conductance that would otherwise occur. However, the Hydraulic Limitation Hypothesis (HLH) has led many biologists to think that in tall trees, pathlength and gravity effects make treetop conditions severe enough that development can no longer produce sufficient conduit dimensions or numbers to sustain water transport, photosynthesis and growth (*9*, *18–21*). If this were generally the case, as trees near their maximum heights, they should show consistent declines in leaf water supply and increasing vulnerability to drought with height. Yet little evidence supports this, because direct tests at the top of tall trees are rare due to the difficulty of reaching treetops over a wide range of heights.

Metabolic scaling theory (*11*, *16*, *17*) predicts that vessel diameters (D) scale with distance from the branch tip (L) following $D \sim aL^b$, with an exponent (b) of 0.2 or above mitigating the resistance increases with increasing path length (*13*, *22*). Insufficient tip-to-base vessel widening (exponent <0.2) would prevent sufficient water flow to the crown, meaning the leaves of tall trees would not stay well hydrated, even under non-drought conditions (*20*, *21*, *23*). Yet, even with an exponent >0.2, recent studies suggest that trees must still adjust other anatomical properties with tree height, such as increasing vessel length, intervessel connectivity (*24*) and vessel diameter and frequency in terminal branches (*15*, *17*). These alternative ways of increasing woody conductance, termed ultra-widening permeability increases, are hypothesized to facilitate isometric scaling between leaf area and active sapwood volume, minimizing drops in conductance and the carbon cost of maintaining significant amounts of additional sapwood with height growth (*15*). However, wider, longer vessels are widely accepted to cause increased vulnerability to conduction-blocking gas embolisms (i.e. the safety-efficiency trade-off; (*6*, *25–28*)), yet this is supported by very little evidence, particularly for tall trees. Data on tip-to-base vessel diameter widening, xylem anatomy and hydraulic traits are crucial, yet especially lacking for very tall trees, leaving a fundamental gap in our understanding of their hydraulic functioning (*12*).

Considering that the average P_{50} (the pressure at which 50% of the xylem hydraulic conductance is lost due to embolism) of a tropical tree is likely to range from -2 to -2.7 MPa (*29*, *30*), gravity alone, which increases xylem tension with height by 9.8 kPa m^{-1}, may considerably reduce the hydraulic safety margin (HSM; the difference between minimum leaf water potential and P_{50}) of taller trees. The effect of gravity cannot be compensated for by vessel diameter adjustments, so gravity-induced declines in water potentials may cause stomatal closure, reduced leaf turgor and negative HSMs (*18–20*, *25*, *31–33*). If gravity reduces hydraulic safety, key hydraulic thresholds, such as leaf turgor loss point (TLP; the water potential at which the leaf loses turgor and stomata fully close) should decline, minimizing the impact of gravity-related declines in leaf water potential on leaf functioning (*21*). Similarly, P_{50} could decline with height to maintain the HSM. Yet, environmental conditions inside large tree crowns are highly context-dependent in response to changes in light availability and evaporative demand (*34*, *35*). It is possible therefore that hydraulic traits are driven not only by increasing tree size but also by vertical canopy-level environmental gradients. This makes predicting trait changes in response to tree height complex, necessitating comprehensive datasets of wood and leaf hydraulic traits and xylem anatomical traits all collected at standard distances from the apical branch tip (*12*). Unfortunately, these datasets are rare and to our knowledge do not exist for tall trees anywhere globally.

This lack of data has led to taller trees being assumed to be more prone to drought-induced mortality, as wider vessels in taller trees are supposed to be less resistance to embolism (*32*). Yet little evidence supports this, as embolism resistance can increase, decrease, or remain unchanged with height (*36–38*). Furthermore, evidencing that height-related changes to a tree's hydraulic system causes drought-related mortality is challenging and requires looking within populations or species to remove the effect of changes in abundance of trees with different sizes and mortality rates across forests (*2*). As large, tall, trees often occur at densities of <10 individuals per hectare, this requires tracking mortality rates at scales larger than most forests inventories. Combining height-related changes in other performance metrics (e.g. growth) with shifts in hydraulic traits likely represents a better way to detect a link between height and mortality risk.

Here we test whether the hydraulic system of very tall tropical tree species is negatively impacted by increases in height. We focus on the tallest known angiosperm tree family, the Dipterocarpaceae, which is dominant in SE Asia's rain forests (*39*). We measured 25 traits related to hydraulic function (water status, leaf pressure-volume relations, embolism resistance, safety margins, xylem anatomy, leaf and wood traits; see Table S1 for units and acronyms) across 38 individual trees of five dipterocarp species, during a non-drought year. We measured traits at multiple positions along each tree (at the base of the trunk and on a lower, a middle, and an upper branch in the crown) on trees ranging from 7.7 to 71 m in height (Fig. S1). The distance between the lower and upper branches sampled exceeded 25 m, close to the mean canopy height of an Amazonian forest, providing a unique opportunity to detect changes in tree function with height. We also measured high-resolution trunk diameter growth rates before, during, and after the strong El Niño drought period of 2023-2024. Using these data we evaluated whether tall trees show systematic drops in water supply to their leaves and concomitant increase in vulnerability to embolism, alongside reductions in growth by testing: i) whether tip-to-base vessel widening prevents longer path lengths causing declines in water potential; ii) whether gravity-induced declines in water potential with height lead to the tallest trees and branches being close to critical hydraulic thresholds, and iii) whether taller trees have greater growth declines than shorter trees during a strong El Niño drought event.

Vessel widening, gravity and leaf water potentials

Height-related increases in hydraulic resistance were likely fully compensated for by vessel diameter widening with increasing tree height (Fig. 1; Fig. S2). Vessel diameters at the base of the trunk were on average significantly ($p < 0.001$) wider in taller trees, with a 70 m tree having vessels 2.2 times wider at the base than a 10 m tree (Fig. 1A). Tip-to-base vessel diameter widening across all trees scaled with distance from the branch tip with an exponent of 0.30 ± 0.04 (0.29 – 0.32 95% confidence interval; Fig. 1B). This is greater than the minimum exponent of 0.2 predicted by metabolic scaling theory to minimize increases in resistance with path length (*11*, *14*). Although uncertainty remains over whether an exponent >0.2 fully compensates for the increase in resistance with path length (*15*, *16*, *25*), it is unlikely that the trees sampled experience significant decreases in hydraulic conductance with height.

If unit-leaf conductance declined with height, we would expect to see a decrease in leaf-specific hydraulic conductivity (K_{sleaf}). Alternatively, some authors posit a reduction in leaf area to sapwood area ratio can maintain a constant leaf water supply capacity, at the cost of higher sapwood volume per leaf area. In trees >7 m tall, we observe no height-related changes in the ratio of leaf area to sapwood area measured at the branch-scale or K_{sleaf}, either within a tree's crown or across individuals of different heights (Table S2; Table S3). It is possible that reduced leaf area occurred at the whole tree scale via branch shedding; however, our vessel scaling data suggests isometric scaling between leaf area and active sapwood volume with tree height (*15*). This is

because a greater slope in the height to vessel diameter relationship across individuals (0.4, Fig. 1A) than within individuals (0.3, Fig. 1B) supports the ultra-widening permeability hypothesis (*15*) (Fig S2). Taken together, our results suggest these trees are likely to be fully compensating for the increases in hydraulic resistance with height through xylem anatomical adjustments.

Declines in leaf water potential with tree height were caused exclusively by gravity (Fig. 2). As expected, upper-crown predawn and midday leaf water potentials became more negative with tree height, in conformity with the gravity-induced hydrostatic gradient (Fig. 2A and 2C). When the effect of gravity (hydrostatic gradient) was removed from the leaf water potential values, the relationship between water potential and height was lost (Fig. 2B). We note a lower sample number at pre-dawn may have introduced bias into our results. However, at midmorning, when transpiration and VPD were low (0.7 ± 0.4 kPa), and when samples could be taken more easily than at pre-dawn, we also found that leaf water potential declined in line with the hydrostatic gradient (-10 ± 4 kPa m^{-1}; Table S2). Midday leaf water potentials also remained close to zero (-1.20 ± 0.50 MPa), only going below -2 MPa in one of the 15 trees that were >50 m tall (Fig. 2A). Foliar leaf water uptake may be contributing to higher-than-expected midday leaf water potentials, as many trees had water potential values that exceeded theoretical limits given the effect of gravity (i.e., points above the hydrostatic gradient; Fig. 2C). Therefore, our data suggests that these trees have evolved multiple strategies that keep their leaves hydrated, even as they grow tall.

In lower and middle crown branches, which are not exposed to the same extremes of light, temperature and VPD, we did not observe the same declines in leaf water potential with height as those found in top crown branches (Fig. 2A-C; Table S4). These results suggest that canopy position may have a more important effect on water potential than tree height in shaded branches of the lower and middle crown, possibly because reduced light availability and complex VPD changes restricts leaf function more than restrictions in stomatal gas exchange (*40*). In addition, lower and middle crown branches were sampled across a narrower range of heights (see Methods), which may limit our ability to detect a signal.

Hydraulic trait adjustments compensate for gravity

Gravity-induced declines in water potential were compensated for by taller trees being more resistant to losses of cell turgor with height. We observed a significant decline in TLP with branch height in the upper canopy (-9 ± 2 kPa m^{-1}; Fig. 2D). The declines in TLP with height resulted in the turgor safety margin being constant with height (intercept of 0.41 ± 0.12 MPa; Fig. 2G; Table S2). Declines in TLP were driven almost exclusively by osmotic adjustments with height (-7 ± 2 kPa m^{-1}; Table S2), which we attributed to osmolyte concentrations in the leaves adjusting with height to maintain turgor at more negative water potentials (*21*). This is supported by the fact that in trees tall enough to be fully sun-exposed (>36 m), we observed no increases in leaf mass per area (LMA) with height (Fig. S3). This suggests height is not directly causing increases in LMA, which should occur if low turgor pressure affects leaf size development (*21*). Therefore, it is likely that there are limited or no height-driven turgor-related restrictions on leaf function in these trees (*19*, *23*).

In addition to maintenance of turgor with height, we observed no changes in branch P_{50} and HSM with height, either within individual trees or between trees of different heights (Figure 2F, 2I; Fig. S4). We did observe a decline in leaf HSM with height in the upper crown branches (-10 ± 5 kPa m^{-1}, $p = 0.044$, Figure 2H). However, this signal was driven by one species (*Dipterocarpus caudiferus*), which had a strong and significant decline of leaf HSM with height (Fig. S5, Table S2). Like most other studies in tropical regions (*30*, *37*, *41*, *42*), our leaf water potential data were measured at the driest point of a normal, non-drought, year, and therefore they do not reflect the absolute minimum HSM during a drought. Yet, our data do show that height growth alone and the

decline in leaf water potential associated with this do not cause a reduction in HSM that predisposes tall trees to be more vulnerable to hydraulic failure.

When considering the difference between the upper and lower crown branch trait values, none of the traits show change with tree height or the change in height between branches, other than leaf HSM and TLP HSM (Fig. S4). The only traits that differed consistently between upper and lower crown branches were branch P_{50} and P_{88} (the pressure at which 88% of the xylem is embolized). Upper crown branches had more negative P_{50} and P_{88} values than lower crown branches (Fig. S4F, Table S3), but this shift was independent of the height difference between the branches ($p = 0.34$). This decline in P_{50} with increasing canopy position and the lack of a safety-efficiency tradeoff (Fig. S6) contradicts the notion that hydraulic safety declines as trees grow taller (*26*, *32*, *41*). These results suggest that changes in embolism resistance and HSM are more likely to be related to branch position within the forest canopy (e.g., light and VPD changes) than height.

Changes in tree growth are independent of tree size during drought

High-resolution tree trunk diameter growth rates for 42 dipterocarps did not show any greater declines in growth in taller than shorter trees, either before or during a strong El Niño related drought (Fig. 3A). During this drought period (December 2023 to May 2024), maximum climatological water deficit (MCWD) was 100 mm, in contrast to 26 mm the previous year, mean precipitation was 35% lower than the long-term mean, mean temperatures were 1.6 ºC higher, and mean VPD was 30% greater, leading to significant soil drying (Fig. 3A and Fig. S7). We note that our growth reference year (July 2022-2023) had slightly greater temperatures and VPD relative to the previous year when traits data were collected (Fig. S7), making it a slightly drier than average year, but this did not translate into significant soil water deficit due to high rainfall. Based on the climatic time series since 1950, a drought with equivalent intensity to the 2023-2024 drought, in terms of changes in VPD, MCWD and temperature, occurs once or twice every century.

Our data during the strong drought year show that changes in tree diameter growth rates were independent of tree height. Comparing the drought year to the growth reference year, only 18 out of 42 trees had reduced growth rates during the drought year (Fig. 3B). However, these 18 trees were not the tallest individuals, and reductions in growth did not correlate with tree height ($p = 0.21$). The remaining 24 trees had no change or even a more pronounced growth in the strong drought year, which may have been a response to a slightly elevated light availability (*43*). Interestingly, the greatest mean reduction in growth occurred during the recovery phase, where 27 trees had lower growth rates and mean growth rate was 22.3% lower than in the same period in the previous wet year ($p = 0.02$; Fig. 3C). Nevertheless, this reduction in diameter growth rate was also unrelated to tree height ($p = 0.58$), with equal reductions in diameter growth across all tree size classes. The lack of relationship between reductions in diameter growth and tree height, and the high variability in tree diameter growth responses to the drought suggests responses to drought are highly variable among individual dipterocarp trees, and that these are not related to tree size. This result is supported by the absence of an effect of tree height on the sensitivity of tree diameter growth rate to soil water content (Fig. S8). Tree height did reduce mean RGR by 1.2 $mm^2\ m^{-2}\ day^{-1}$ ($p = 0.01$), but this is likely an artefact of the way RGR is calculated relative to basal area. Taller trees increase their basal area by accumulating heartwood, while sapwood does not increase to the same proportion, especially in the very large trees studied here.

Implications and conclusions

Our study is consistent with natural selection in giant broadleaf trees favoring adjustments in xylem anatomy and leaf hydraulic properties with height that fully compensate for the effects of

gravity and path length as they get taller. This means leaf water supply and function is not reduced in tall trees during regular climatic conditions, suggesting both tall and short trees may have a similar capacity to accommodate drought. Similarly, we show these tall trees have no reductions in embolism resistance with height and also suffer no greater declines in growth during a strong drought than smaller individuals of the same species. However, our results show that through these deep, complex canopies hydraulic trait changes may be more related to canopy-driven shifts in microclimatic conditions, shading and photosynthetic optimization, than to height (*44*, *45*). For example, declines in leaf nutrient concentrations, LMA and photosynthetic capacity from sun to shade leaves are common in these dipterocarp trees (*46*, *47*), necessitating different photosynthetic strategies with shifts in canopy position. Top crown leaves of more exposed trees, irrespective of height, would have lower leaf water potentials, which would reduce stomatal conductance. The adaptation to have lower P_{50} in the upper canopy branches (Fig. S3F) reduces the embolism risk, thus minimizing the need for stomatal closure (*46*, *47*). Costly adaptations to lower P_{50} are not needed in shaded parts of the canopy where water potentials are lower (*47*). These results suggest we need to view tall trees as functionally differentiated organisms, with an ecological strategy that is defined not by a mean set of traits, but by their capacity to quasi-independently adjust traits between sectors in response to microclimate conditions.

Trees taller than those we measured may suffer height-related hydraulic damage, as some individuals in these forests can attain statures up to 100 m (*48*). Trees above 70m tall are, however, extremely rare (Fig. S9), and make up only a small proportion of total carbon stocks. Whether xylem anatomical adjustments and changes in TLP, or other trait changes, compensate for the effects of path length and gravity in other large tropical trees, such as those found in Amazonia (*49*), or in tall temperate trees, remains to be explored. To our knowledge no other study exists on giant trees within or outside of the tropics that standardizes anatomical and trait measurements from the apex throughout the canopy. Therefore, it is possible the conclusions from our study may be more generally relevant to tall trees. Critically, however, our study shows that the widely adopted assumption of increased hydraulic vulnerability with tree size needs to be more widely verified (*50*) and should not be assumed to explain the elevated mortality in taller trees (*4*, *6*, *51*, *52*).

References and Notes

1. J. A. Lutz, T. J. Furniss, D. J. Johnson, S. J. Davies, D. Allen, A. Alonso, K. J. Anderson-Teixeira, A. Andrade, J. Baltzer, K. M. L. Becker, E. M. Blomdahl, N. A. Bourg, S. Bunyavejchewin, D. F. R. P. Burslem, C. A. Cansler, K. Cao, M. Cao, D. Cárdenas, L. Chang, K. Chao, W. Chao, J. Chiang, C. Chu, G. B. Chuyong, K. Clay, R. Condit, S. Cordell, H. S. Dattaraja, A. Duque, C. E. N. Ewango, G. A. Fischer, C. Fletcher, J. A. Freund, C. Giardina, S. J. Germain, G. S. Gilbert, Z. Hao, T. Hart, B. C. H. Hau, F. He, A. Hector, R. W. Howe, C. Hsieh, Y. Hu, S. P. Hubbell, F. M. Inman-Narahari, A. Itoh, D. Janík, A. R. Kassim, D. Kenfack, L. Korte, K. Král, A. J. Larson, Y. Li, Y. Lin, S. Liu, S. Lum, K. Ma, J. Makana, Y. Malhi, S. M. McMahon, W. J. McShea, H. R. Memiaghe, X. Mi, M. Morecroft, P. M. Musili, J. A. Myers, V. Novotny, A. De Oliveira, P. Ong, D. A. Orwig, R. Ostertag, G. G. Parker, R. Patankar, R. P. Phillips, G. Reynolds, L. Sack, G. M. Song, S. Su, R. Sukumar, I. Sun, H. S. Suresh, M. E. Swanson, S. Tan, D. W. Thomas, J. Thompson, M. Uriarte, R. Valencia, A. Vicentini, T. Vrška, X. Wang, G. D. Weiblen, A. Wolf, S. Wu, H. Xu, T. Yamakura, S. Yap, J. K. Zimmerman, Global importance of large-diameter trees. *Global Ecol Biogeogr* **27**, 849–864 (2018).

2. N. L. Stephenson, A. J. Das, Height-related changes in forest composition explain increasing tree mortality with height during an extreme drought. *Nat Commun* **11**, 3402 (2020).

3. J. W. F. Slik, G. Paoli, K. McGuire, I. Amaral, J. Barroso, M. Bastian, L. Blanc, F. Bongers, P. Boundja, C. Clark, M. Collins, G. Dauby, Y. Ding, J. Doucet, E. Eler, L. Ferreira, O. Forshed, G. Fredriksson, J. Gillet, D. Harris, M. Leal, Y. Laumonier, Y. Malhi, A. Mansor, E. Martin, K. Miyamoto, A. Araujo-Murakami, H. Nagamasu, R. Nilus, E. Nurtjahya, Á. Oliveira, O. Onrizal, A. Parada-Gutierrez, A. Permana, L. Poorter, J. Poulsen, H. Ramirez-Angulo, J. Reitsma, F. Rovero, A. Rozak, D. Sheil, J. Silva-Espejo, M. Silveira, W. Spironelo, H. Ter Steege, T. Stevart, G. E. Navarro-Aguilar, T. Sunderland, E. Suzuki, J. Tang, I. Theilade, G. Van Der Heijden, J. Van Valkenburg, T. Van Do, E. Vilanova, V. Vos, S. Wich, H. Wöll, T. Yoneda, R. Zang, M. Zhang, N. Zweifel, Large trees drive forest aboveground biomass variation in moist lowland forests across the tropics. *Global Ecology and Biogeography* **22**, 1261–1271 (2013).

4. E. M. Gora, A. Esquivel-Muelbert, Implications of size-dependent tree mortality for tropical forest carbon dynamics. *Nat. Plants* **7**, 384–391 (2021).

5. W. Hubau, S. L. Lewis, O. L. Phillips, K. Affum-Baffoe, H. Beeckman, A. Cuní-Sanchez, A. K. Daniels, C. E. N. Ewango, S. Fauset, J. M. Mukinzi, D. Sheil, B. Sonké, M. J. P. Sullivan, T. C. H. Sunderland, H. Taedoumg, S. C. Thomas, L. J. T. White, K. A. Abernethy, S. Adu-Bredu, C. A. Amani, T. R. Baker, L. F. Banin, F. Baya, S. K. Begne, A. C. Bennett, F. Benedet, R. Bitariho, Y. E. Bocko, P. Boeckx, P. Boundja, R. J. W. Brienen, T. Brncic, E. Chezeaux, G. B. Chuyong, C. J. Clark, M. Collins, J. A. Comiskey, D. A. Coomes, G. C. Dargie, T. De Haulleville, M. N. D. Kamdem, J.-L. Doucet, A. Esquivel-Muelbert, T. R. Feldpausch, A. Fofanah, E. G. Foli, M. Gilpin, E. Gloor, C. Gonmadje, S. Gourlet-Fleury, J. S. Hall, A. C. Hamilton, D. J. Harris, T. B. Hart, M. B. N. Hockemba, A. Hladik, S. A. Ifo, K. J. Jeffery, T. Jucker, E. K. Yakusu, E. Kearsley, D. Kenfack, A. Koch, M. E. Leal, A. Levesley, J. A. Lindsell, J. Lisingo, G. Lopez-Gonzalez, J. C. Lovett, J.-R. Makana, Y. Malhi, A. R. Marshall, J. Martin, E. H. Martin, F. M. Mbayu, V. P. Medjibe, V. Mihindou, E. T. A. Mitchard, S. Moore, P. K. T. Munishi, N. N. Bengone, L. Ojo, F. E. Ondo, K. S.-H. Peh, G. C. Pickavance, A. D. Poulsen, J. R. Poulsen, L. Qie, J. Reitsma, F. Rovero, M. D. Swaine, J. Talbot, J. Taplin, D. M. Taylor, D. W. Thomas, B. Toirambe, J. T. Mukendi, D. Tuagben, P. M. Umunay, G. M. F. Van Der Heijden, H. Verbeeck, J. Vleminckx, S. Willcock, H. Wöll, J. T. Woods, L. Zemagho, Asynchronous carbon sink saturation in African and Amazonian tropical forests. *Nature* **579**, 80–87 (2020).

6. A. C. Bennett, N. G. McDowell, C. D. Allen, K. J. Anderson-Teixeira, Larger trees suffer most during drought in forests worldwide. *Nature Plants* **1**, 15139 (2015).

7. A. E. L. Stovall, H. Shugart, X. Yang, Tree height explains mortality risk during an intense drought. *Nat Commun* **10**, 4385 (2019).

8. P. Cruiziat, H. Cochard, T. Améglio, Hydraulic architecture of trees: main concepts and results. *Annals of forest science* **59**, 723–752 (2002).

9. M. G. Ryan, N. Phillips, B. J. Bond, The hydraulic limitation hypothesis revisited. *Plant Cell & Environment* **29**, 367–381 (2006).

10. A. Segovia-Rivas, M. E. Olson, Temperature and Turgor "Limitation" and Environmental "Control" in Xylem Biology and Dendrochronology. *Integrative And Comparative Biology* **63**, 1364–1375 (2023).

11. G. B. West, J. H. Brown, B. J. Enquist, A general model for the structure and allometry of plant vascular systems. *Nature* **400**, 664–667 (1999).

12. M. E. Olson, T. Anfodillo, S. M. Gleason, K. A. McCulloh, Tip-to-base xylem conduit widening as an adaptation: causes, consequences, and empirical priorities. *New Phytologist*, doi: 10.1111/nph.16961 (2020).

13. T. Anfodillo, V. Carraro, M. Carrer, C. Fior, S. Rossi, Convergent tapering of xylem conduits in different woody species. *New Phytologist* **169**, 279–290 (2006).

14. G. Petit, T. Anfodillo, Plant physiology in theory and practice: An analysis of the WBE model for vascular plants. *Journal of Theoretical Biology* **259**, 1–4 (2009).

15. T. Anfodillo, M. E. Olson, Stretched sapwood, ultra-widening permeability and ditching da Vinci: revising models of plant form and function. *Annals of Botany* **134**, 19–42 (2024).

16. B. J. Enquist, Universal scaling in tree and vascular plant allometry: toward a general quantitative theory linking plant form and function from cells to ecosystems. *Tree Physiology* **22**, 1045–1064 (2002).

17. V. M. Savage, L. P. Bentley, B. J. Enquist, J. S. Sperry, D. D. Smith, P. B. Reich, E. I. von Allmen, Hydraulic trade-offs and space filling enable better predictions of vascular structure and function in plants. *Proceedings of the National Academy of Sciences* **107**, 22722–22727 (2010).

18. M. G. Ryan, B. J. Yoder, Hydraulic Limits to Tree Height and Tree Growth. *BioScience* **47**, 235–242 (1997).

19. G. W. Koch, S. C. Sillett, G. M. Jennings, S. D. Davis, The limits to tree height. *Nature* **428**, 851–854 (2004).

20. S. S. O. Burgess, T. E. Dawson, Predicting the limits to tree height using statistical regressions of leaf traits. *New Phytologist* **174**, 626–636 (2007).

21. D. R. Woodruff, B. J. Bond, F. C. Meinzer, Does turgor limit growth in tall trees? *Plant, Cell & Environment* **27**, 229–236 (2004).

22. M. E. Olson, R. Aguirre-Hernández, J. A. Rosell, Universal foliage-stem scaling across environments and species in dicot trees: plasticity, biomechanics and Corner's Rules. *Ecology Letters* **12**, 210–219 (2009).

23. S. S. O. Burgess, J. Pittermann, T. E. Dawson, Hydraulic efficiency and safety of branch xylem increases with height in *Sequoia sempervirens* (D. Don) crowns. *Plant Cell & Environment* **29**, 229–239 (2006).

24. S. Kreinert, L. Kaack, L. Pereira, M. Miranda, S. Mäck, J. Schuler, S. Jansen, Xylem conduit dimensions show no hydraulic bottleneck along the axis of an angiosperm tree. Preprints [Preprint] (2025). https://doi.org/10.22541/au.174298901.16137246/v1.

25. M. Mencuccini, Hydraulic constraints in the functional scaling of trees. *Tree Physiology* **22**, 553–565 (2002).

26. L. Rowland, A. C. L. da Costa, D. R. Galbraith, R. S. Oliveira, O. J. Binks, A. A. R. Oliveira, A. M. Pullen, C. E. Doughty, D. B. Metcalfe, S. S. Vasconcelos, L. V. Ferreira, Y. Malhi, J. Grace, M. Mencuccini, P. Meir, Death from drought in tropical forests is triggered by hydraulics not carbon starvation. *Nature*, doi: 10.1038/nature15539 (2015).

27. H. Liu, S. M. Gleason, G. Hao, L. Hua, P. He, G. Goldstein, Q. Ye, Hydraulic traits are coordinated with maximum plant height at the global scale. *Science Advances* **5**, eaav1332 (2019).

28. N. McDowell, H. Barnard, B. Bond, T. Hinckley, R. Hubbard, H. Ishii, B. Köstner, F. Magnani, J. Marshall, F. Meinzer, N. Phillips, M. Ryan, D. Whitehead, The relationship between tree height and leaf area: sapwood area ratio. *Oecologia* **132**, 12–20 (2002).

29. C. M. Smith-Martin, R. Muscarella, W. M. Hammond, S. Jansen, T. J. Brodribb, B. Choat, D. M. Johnson, G. Vargas-G, M. Uriarte, Hydraulic variability of tropical forests is largely independent of water availability. *Ecology Letters* **26**, 1829–1839 (2023).

30. J. V. Tavares, R. S. Oliveira, M. Mencuccini, C. Signori-Müller, L. Pereira, F. C. Diniz, M. Gilpin, M. J. Marca Zevallos, C. A. Salas Yupayccana, M. Acosta, F. M. Pérez Mullisaca, F. D. V. Barros, P. Bittencourt, H. Jancoski, M. C. Scalon, B. S. Marimon, I. Oliveras Menor, B. H. Marimon, M. Fancourt, A. Chambers-Ostler, A. Esquivel-Muelbert, L. Rowland, P. Meir, A. C. Lola Da Costa, A. Nina, J. M. B. Sanchez, J. S. Tintaya, R. S. C. Chino, J. Baca, L. Fernandes, E. R. M. Cumapa, J. A. R. Santos, R. Teixeira, L. Tello, M. T. M. Ugarteche, G. A. Cuellar, F. Martinez, A. Araujo-Murakami, E. Almeida, W. J. A. Da Cruz, J. Del Aguila Pasquel, L. Aragão, T. R. Baker, P. B. De Camargo, R. Brienen, W. Castro, S. C. Ribeiro, F. Coelho De Souza, E. G. Cosio, N. Davila Cardozo, R. Da Costa Silva, M. Disney, J. S. Espejo, T. R. Feldpausch, L. Ferreira, L. Giacomin, N. Higuchi, M. Hirota, E. Honorio, W. Huaraca Huasco, S. Lewis, G. Flores Llampazo, Y. Malhi, A. Monteagudo Mendoza, P. Morandi, V. Chama Moscoso, R. Muscarella, D. Penha, M. C. Rocha, G. Rodrigues, A. R. Ruschel, N. Salinas, M. Schlickmann, M. Silveira, J. Talbot, R. Vásquez, L. Vedovato, S. A. Vieira, O. L. Phillips, E. Gloor, D. R. Galbraith, Basin-wide variation in tree hydraulic safety margins predicts the carbon balance of Amazon forests. *Nature* **617**, 111–117 (2023).

31. M. Mencuccini, J. Grace, Hydraulic conductance, light interception and needle nutrient concentration in Scots pine stands and their relations with net primary productivity. *Tree Physiology* **16**, 459–468 (1996).

32. J. S. Sperry, F. C. Meinzer, K. a McCulloh, Safety and efficiency conflicts in hydraulic architecture: scaling from tissues to trees. *Plant, cell & environment* **31**, 632–45 (2008).

33. A. Potkay, T. Hölttä, A. T. Trugman, Y. Fan, Turgor-limited predictions of tree growth, height and metabolic scaling over tree lifespans. *Tree Physiology* **42**, 229–252 (2022).

34. Ü. Niinemets, A review of light interception in plant stands from leaf to canopy in different plant functional types and in species with varying shade tolerance. *Ecological Research* **25**, 693–714 (2010).

35. D. M. A. Rozendaal, V. H. Hurtado, L. Poorter, Plasticity in leaf traits of 38 tropical tree species in response to light; relationships with light demand and adult stature. *Functional Ecology* **20**, 207–216 (2006).

36. P. R. de L. Bittencourt, D. C. Bartholomew, L. F. Banin, M. A. F. Bin Suis, R. Nilus, D. F. R. P. Burslem, L. Rowland, Divergence of hydraulic traits among tropical forest trees across topographic and vertical environment gradients in Borneo. *New Phytologist* **235**, 2183–2198 (2022).

37. P. R. L. Bittencourt, R. S. Oliveira, A. C. L. da Costa, A. L. Giles, I. Coughlin, P. B. Costa, D. C. Bartholomew, L. V. Ferreira, S. S. Vasconcelos, F. V. Barros, J. A. S. Junior, A. A. R. Oliveira, M. Mencuccini, P. Meir, L. Rowland, Amazonian trees have limited capacity to acclimate plant hydraulic properties in response to long-term drought. *Global Change Biology*, doi: 10.1111/gcb.15040 (2020).

38. L. Fernández-de-Uña, J. Martínez-Vilalta, R. Poyatos, M. Mencuccini, N. G. McDowell, The role of height-driven constraints and compensations on tree vulnerability to drought. *New Phytologist* **239**, 2083–2098 (2023).

39. P. Ashton, *On the Forests of Tropical Asia: Lest the Memory Fade* (Kew publishing, Richmond (GB), 2015).

40. T. Sibret, M. Peaucelle, K. Y. Crous, F. Meunier, M. Bauters, D. S. Ellsworth, I. A. Janssens, P. Boeckx, H. Verbeeck, Photosynthetic traits scale linearly with relative height within the canopy in an African tropical forest. *New Phytologist* **246**, 2029–2045 (2025).

41. I. Araújo, B. S. Marimon, B. H. M. Junior, C. H. L. Oliveira, J. W. S. Silva, R. G. Beú, I. V. Da Silva, P. F. Simioni, J. V. Tavares, O. L. Phillips, M. U. Gloor, D. R. Galbraith, Taller trees exhibit greater hydraulic vulnerability in southern Amazonian forests. *Environmental and Experimental Botany* **226**, 105905 (2024).

42. F. de V. Barros, P. R. L. Bittencourt, M. Brum, N. Restrepo-Coupe, L. Pereira, G. S. Teodoro, S. R. Saleska, L. S. Borma, B. O. Christoffersen, D. Penha, L. F. Alves, A. J. N. Lima, V. M. C. Carneiro, P. Gentine, J. Lee, L. E. O. C. Aragão, V. Ivanov, L. S. M. Leal, A. C. Araujo, R. S. Oliveira, Hydraulic traits explain differential responses of Amazonian forests to the 2015 El Niño-induced drought. *New Phytologist* **223**, 1253–1266 (2019).

43. M. H. Nunes, S. Both, B. Bongalov, C. Brelsford, S. Khoury, D. F. R. P. Burslem, C. Philipson, N. Majalap, T. Riutta, D. A. Coomes, M. E. J. Cutler, Changes in leaf functional traits of rainforest canopy trees associated with an El Niño event in Borneo. *Environ. Res. Lett.* **14**, 085005 (2019).

44. C. O. Marks, M. J. Lechowicz, Alternative Designs and the Evolution of Functional Diversity. *The American Naturalist* **167**, 55–66 (2006).

45. G. P. Asner, R. E. Martin, Canopy phylogenetic, chemical and spectral assembly in a lowland Amazonian forest. *New Phytologist* **189**, 999–1012 (2011).

46. D. C. Bartholomew, L. F. Banin, P. R. L. Bittencourt, M. A. F. Suis, L. M. Mercado, R. Nilus, D. F. R. P. Burslem, L. Rowland, Differential nutrient limitation and tree height control leaf physiology, supporting niche partitioning in tropical dipterocarp forests. *Functional Ecology* **36**, 2084–2103 (2022).

47. T. Kenzo, Y. Inoue, M. Yoshimura, M. Yamashita, A. Tanaka-Oda, T. Ichie, Height-related changes in leaf photosynthetic traits in diverse Bornean tropical rain forest trees. *Oecologia* **177**, 191–202 (2015).

48. A. Shenkin, C. J. Chandler, D. S. Boyd, T. Jackson, M. Disney, N. Majalap, R. Nilus, G. Foody, J. bin Jami, G. Reynolds, P. Wilkes, M. E. J. Cutler, G. M. F. van der Heijden, D. F. R. P. Burslem, D. A. Coomes, L. P. Bentley, Y. Malhi, The World's Tallest Tropical Tree in Three Dimensions. *Frontiers in Forests and Global Change* **2** (2019).

49. E. B. Gorgens, A. Z. Motta, M. Assis, M. H. Nunes, T. Jackson, D. Coomes, J. Rosette, L. E. O. e C. Aragão, J. P. Ometto, The giant trees of the Amazon basin. *Front Ecol Environ* **17**, 373–374 (2019).

50. L. Fernández-de-Uña, J. Martínez-Vilalta, R. Poyatos, M. Mencuccini, N. G. McDowell, The role of height-driven constraints and compensations on tree vulnerability to drought. *New Phytologist* **239**, 2083–2098 (2023).

51. O. L. Phillips, G. Van Der Heijden, S. L. Lewis, G. López-González, L. E. Aragão, J. Lloyd, Y. Malhi, A. Monteagudo, S. Almeida, E. A. Dávila, others, Drought–mortality relationships for tropical forests. *New Phytologist* **187**, 631–646 (2010).

52. N. G. McDowell, C. D. Allen, K. Anderson-Teixeira, B. H. Aukema, B. Bond-Lamberty, L. Chini, J. S. Clark, M. Dietze, C. Grossiord, A. Hanbury-Brown, G. C. Hurtt, R. B. Jackson, D. J. Johnson, L. Kueppers, J. W. Lichstein, K. Ogle, B. Poulter, T. A. M. Pugh, R. Seidl, M. G. Turner, M. Uriarte, A. P. Walker, C. Xu, Pervasive shifts in forest dynamics in a changing world. *Science* **368**, eaaz9463 (2020).

53. P. Bittencourt, A. Scheire, P. Jotan, J. Lourenço-Junior, L. Banin, Mohd. A. F. bin Suis, D. F. R. P. Burslem, B. Christoffersen, D. Coomes, P. Groenendijk, S. Jansen, T. Jucker, R. Matula, M. Mencuccini, R. Oliveira, R. Plichta, R. Nilus, R. Robert, M. Svátek, L. Rowland, Functional traits of the tallest tropical tree species in Borneo, 2022. doi: 10.5285/6ECFD160-4740-491E-A8B3-8CBB3A4C8701 (2026).

54. P. Bittencourt, A. Scheire, P. Jotan, J. Lourenço-Junior, L. Banin, Mohd. A. F. bin Suis, D. F. R. P. Burslem, B. Christoffersen, D. Coomes, P. Groenendijk, S. Jansen, T. Jucker, R. Matula, M. Mencuccini, R. Oliveira, R. Plichta, R. Nilus, R. Robert, M. Svátek, L. Rowland, Height does not impair the hydraulic system of the tallest tropical Dipterocarp trees. doi: https://doi.org/10.5061/dryad.d51c5b0j4 (2026).

55. Y. F. Huang, J. L. Ng, K. F. Fung, T. K. Weng, N. AlDahoul, A. N. Ahmed, M. Sherif, B. Chaplot, K. L. Chong, A. Elshafie, Space–time heterogeneity of drought characteristics in Sabah and Sarawak, East Malaysia: implications for developing effective drought monitoring and mitigation strategies. *Appl Water Sci* **13** (2023).

56. M. Nakagawa, K. Tanaka, T. Nakashizuka, T. Ohkubo, T. Kato, T. Maeda, K. Sato, H. Miguchi, H. Nagamasu, K. Ogino, S. Teo, A. A. Hamid, L. H. Seng, Impact of severe drought associated with the 1997–1998 El Niño in a tropical forest in Sarawak. *Journal of Tropical Ecology* **16**, 355–367 (2000).

57. D. M. Newbery, M. Lingenfelder, Resistance of a lowland rain forest to increasing drought intensity in Sabah, Borneo. *J. Trop. Ecol.* **20**, 613–624 (2004).

58. J. W. F. Slik, El Niño droughts and their effects on tree species composition and diversity in tropical rain forests. *Oecologia* **141**, 114–120 (2004).

59. A. Itoh, S. Nanami, T. Harata, T. Ohkubo, S. Tan, L. Chong, S. J. Davies, T. Yamakura, The Effect of Habitat Association and Edaphic Conditions on Tree Mortality during El Niño-induced Drought in a Bornean Dipterocarp Forest. *Biotropica* **44**, 606–617 (2012).

60. K. Miyamoto, S. Aiba, R. Aoyagi, R. Nilus, Effects of El Niño drought on tree mortality and growth across forest types at different elevations in Borneo. *Forest Ecology and Management* **490**, 119096 (2021).

61. M. G. L. Van Nieuwstadt, D. Sheil, Drought, fire and tree survival in a Borneo rain forest, East Kalimantan, Indonesia. *J Ecology* **93**, 191–201 (2005).

62. R. Nilus, Effect of Edaphic Variation on Forest Structure, Dynamics, Diversity and Regeneration in a Lowland Tropical Rain Forest in Borneo. *University of Aberdeen, Aberdeen, UK.* (2004).

63. T. Jucker, B. Bongalov, D. F. R. P. Burslem, R. Nilus, M. Dalponte, S. L. Lewis, O. L. Phillips, L. Qie, D. A. Coomes, Topography shapes the structure, composition and function of tropical forest landscapes. *Ecology Letters*, doi: 10.1111/ele.12964 (2018).

64. P. F. Scholander, H. T. Hammel, E. A. Hemmingsen, E. D. Bradstreet, Hydrostatic pressure and osmotic potential in leaves of mangroves and some other plants. *Proceedings of the National Academy of Sciences of the United States of America* **52**, 119 (1964).

65. L. Pereira, P. R. L. Bittencourt, R. S. Oliveira, M. B. M. Junior, F. V. Barros, R. V. Ribeiro, P. Mazzafera, Plant pneumatics: stem air flow is related to embolism - new perspectives on methods in plant hydraulics. *New Phytologist*, n/a-n/a (2016).

66. L. Pereira, P. R. L. Bittencourt, V. S. Pacheco, M. T. Miranda, Y. Zhang, R. S. Oliveira, P. Groenendijk, E. C. Machado, M. T. Tyree, S. Jansen, L. Rowland, R. V. Ribeiro, The Pneumatron: an automated pneumatic apparatus for estimating xylem vulnerability to embolism at high temporal resolution. *Plant, Cell & Environment*, doi: 10.1111/pce.13647 (2019).

67. P. Bittencourt, L. Pereira, R. Oliveira, Pneumatic Method to Measure Plant Xylem Embolism. *BIO-PROTOCOL* **8** (2018).

68. J. S. Sperry, J. R. Donnelly, M. T. Tyree, A method for measuring hydraulic conductivity and embolism in xylem. *Plant, Cell and Environment* **11**, 35–40 (1988).

69. M. Brum, L. Pereira, R. V. Ribeiro, S. Jansen, P. R. L. Bittencourt, R. S. Oliveira, S. R. Saleska, Reconciling discrepancies in measurements of vulnerability to xylem embolism with the pneumatic method. *New Phytologist* **237**, 374–383 (2023).

70. N. W. Pammenter, C. Vander Willigen, A mathematical and statistical analysis of the curves illustrating vulnerability of xylem to cavitation. *Tree physiology* **18**, 589–593 (1998).

71. B. Choat, T. J. Brodribb, C. R. Brodersen, R. A. Duursma, R. López, B. E. Medlyn, Triggers of tree mortality under drought. *Nature* **558**, 531–539 (2018).

72. M. T. Tyree, H. T. Hammel, The Measurement of the Turgor Pressure and the Water Relations of Plants by the Pressure-bomb Technique. *Journal of Experimental Botany* **23**, 267–282 (1972).

73. P. J. ; H. Schulte, A Comparison of Pressure-Volume Curve Data Analysis Techniques. *Journal of experimental botany* **36**, 1590–1602 (1985).

74. A. Raesch, pvldcurve: Simplifies the Analysis of Pressure Volume and Leaf Drying Curves (2020).

75. T. J. Brodribb, R. P. Skelton, S. A. M. McAdam, D. Bienaimé, C. J. Lucani, P. Marmottant, Visual quantification of embolism reveals leaf vulnerability to hydraulic failure. *New Phytologist*, n/a-n/a (2016).

76. C. A. Schneider, W. S. Rasband, K. W. Eliceiri, NIH Image to ImageJ: 25 years of image analysis. *Nature Methods* **9**, 671–675 (2012).

77. C. Lucani, New and improved techniques for assessing drought tolerance in plants (2019).

78. H. Gärtner, S. Lucchinetti, F. H. Schweingruber, New perspectives for wood anatomical analysis in dendrosciences: The GSL1-microtome. *Dendrochronologia* **32**, 47–51 (2014).

79. J. Jonkman, C. M. Brown, G. D. Wright, K. I. Anderson, A. J. North, Tutorial: guidance for quantitative confocal microscopy. *Nat Protoc* **15**, 1585–1611 (2020).

80. The GIMP Development Team, GIMP (2019). https://www.gimp.org.

81. A. Scholz, M. Klepsch, Z. Karimi, S. Jansen, How to quantify conduits in wood? *Frontiers in Plant Science* **4** (2013).

82. A. E. Zanne, M. Westoby, D. S. Falster, D. D. Ackerly, S. R. Loarie, S. E. J. Arnold, D. A. Coomes, Angiosperm wood structure: Global patterns in vessel anatomy and their relation to wood density and potential conductivity. *American Journal of Botany* **97**, 207–215 (2010).

83. N. Pérez-Harguindeguy, S. Díaz, E. Garnier, S. Lavorel, H. Poorter, P. Jaureguiberry, M. S. Bret-Harte, W. K. Cornwell, J. M. Craine, D. E. Gurvich, C. Urcelay, E. J. Veneklaas, P. B. Reich, L. Poorter, I. J. Wright, P. Ray, L. Enrico, J. G. Pausas, A. C. de Vos, N. Buchmann, G. Funes, F. Quétier, J. G. Hodgson, K. Thompson, H. D. Morgan, H. ter Steege, L. Sack, B. Blonder, P. Poschlod, M. V. Vaieretti, G. Conti, A. C. Staver, S. Aquino, J. H. C. Cornelissen, New handbook for standardised measurement of plant functional traits worldwide. *Australian Journal of Botany* **61**, 167 (2013).

84. M. Katabuchi, LeafArea: an R package for rapid digital image analysis of leaf area. *Ecological Research* **30**, 1073–1077 (2015).

85. J. Wild, M. Kopecký, M. Macek, M. Šanda, J. Jankovec, T. Haase, Climate at ecologically relevant scales: A new temperature and soil moisture logger for long-term microclimate measurement. *Agricultural and Forest Meteorology* **268**, 40–47 (2019).

86. R. Matula, S. Knířová, J. Vítámvás, M. Šrámek, T. Knír, I. Ulbrichová, M. Svoboda, R. Plichta, Shifts in intra-annual growth dynamics drive a decline in productivity of temperate trees in Central European forest under warmer climate. *Science of The Total Environment* **905**, 166906 (2023).

87. S. Etzold, F. Sterck, A. K. Bose, S. Braun, N. Buchmann, W. Eugster, A. Gessler, A. Kahmen, R. L. Peters, Y. Vitasse, L. Walthert, K. Ziemińska, R. Zweifel, Number of growth days and not length of the growth period determines radial stem growth of temperate trees. *Ecology Letters* **25**, 427–439 (2022).

88. Copernicus Climate Change Service, ERA5-Land monthly averaged data from 2001 to present, ECMWF (2019); https://doi.org/10.24381/CDS.68D2BB30.

89. M. Réjou-Méchain, A. Tanguy, C. Piponiot, J. Chave, B. Hérault, BIOMASS : an R package for estimating above-ground biomass and its uncertainty in tropical forests. *Methods Ecol Evol* **8**, 1163–1167 (2017).

90. D. Coomes, T. Jackson, Airborne LiDAR and RGB imagery from Sepilok Reserve and Danum Valley in Malaysia in 2020, NERC EDS Centre for Environmental Data Analysis (2022); https://doi.org/10.5285/DD4D20C8626F4B9D99BC14358B1B50FE.

91. T. Jucker, F. J. Fischer, J. Chave, D. A. Coomes, J. Caspersen, A. Ali, G. J. Loubota Panzou, T. R. Feldpausch, D. Falster, V. A. Usoltsev, S. Adu-Bredu, L. F. Alves, M. Aminpour, I. B. Angoboy, N. P. R. Anten, C. Antin, Y. Askari, R. Muñoz, N. Ayyappan, P. Balvanera, L. Banin, N. Barbier, J. J. Battles, H. Beeckman, Y. E. Bocko, B. Bond-Lamberty, F. Bongers, S. Bowers, T. Brade, M. Van Breugel, A. Chantrain, R. Chaudhary, J. Dai, M. Dalponte, K. Dimobe, J. Domec, J. Doucet, R. A. Duursma, M. Enríquez, K. Y. Van Ewijk, W. Farfán-Rios, A. Fayolle, E. Forni, D. I. Forrester, H. Gilani, J. L. Godlee, S. Gourlet-Fleury, M. Haeni, J. S. Hall, J. He, A. Hemp, J. L. Hernández-Stefanoni, S. I. Higgins, R. J. Holdaway, K. Hussain, L. B. Hutley, T. Ichie, Y. Iida, H. Jiang, P. R. Joshi, H. Kaboli, M. K. Larsary, T. Kenzo, B. D. Kloeppel, T. Kohyama, S. Kunwar, S. Kuyah, J. Kvasnica, S. Lin, E. R. Lines, H. Liu, C. Lorimer, J. Loumeto, Y. Malhi, P. L. Marshall, E. Mattsson, R. Matula, J. A. Meave, S. Mensah, X. Mi, S. Momo, G. R. Moncrieff, F. Mora, S. P. Nissanka, K. L. O'Hara, S. Pearce, R. Pelissier, P. L. Peri, P. Ploton, L. Poorter, M. J. Pour, H. Pourbabaei, J. M. Dupuy-Rada, S. C. Ribeiro, C. Ryan, A. Sanaei, J. Sanger, M. Schlund, G. Sellan, A. Shenkin, B. Sonké, F. J. Sterck, M. Svátek, K. Takagi, A. T. Trugman, F. Ullah, M. A. Vadeboncoeur, A. Valipour, M. C. Vanderwel, A. G. Vovides, W. Wang, L. Wang, C. Wirth, M. Woods, W. Xiang, F. D. A. Ximenes, Y. Xu, T. Yamada, M. A. Zavala, Tallo: A global tree allometry and crown architecture database. *Global Change Biology* **28**, 5254–5268 (2022).

92. R Core Team, R: A language and environment for statistical computing. *R Foundation for Statistical Computing, Vienna, Austria* (2022).

93. A. F. Zuur, E. N. Ieno, N. Walker, A. A. Saveliev, G. M. Smith, *Mixed Effects Models and Extensions in Ecology with R* (Springer New York, New York, NY, 2009; http://link.springer.com/10.1007/978-0-387-87458-6)*Statistics for Biology and Health*.

94. B. Pinheiro, nlme: Linear and Nonlinear Mixed Effects Models. *R package version 3.1-160* (2022).

95. B. Pinheiro, *Mixed-Effects Models in S and S-PLUS* (Springer-Verlag, New York, 2000; http://link.springer.com/10.1007/b98882)*Statistics and Computing*.

96. K. Barton, MuMIn: Multi-Model Inference_. *R package version 1.47.1* (2022).

97. D. Bates, M. Mächler, B. Bolker, S. Walker, Fitting Linear Mixed-Effects Models Using **lme4**. *J. Stat. Soft.* **67** (2015).

98. D. I. Warton, R. A. Duursma, D. S. Falster, S. Taskinen, smatr 3- an R package for estimation and inference about allometric lines: The smatr 3 - an R package. *Methods in Ecology and Evolution* **3**, 257–259 (2012).

99. R. Thomas, I. Vaughan, J. Lello, *Data Analysis with R Statistical Software: A Guidebook for Scientists* (Eco-explore, United Kingdom, 2017).

Acknowledgments: We thank Danielle Leal Ramos (University of Exeter), Mat Disney (University College London) and Toby Jackson (University of Bristol) for their support in the preparation of the printed summary figure. We would also like to thank Mark Olson and two other anonymous reviewers for their highly constructive comments during the review process.

Funding:

UK Natural Environment Research Council grant NE/V000071/1 (LR, PB, DB, LB)

NERC GW4+ studentship (AS)

UK NERC Independent Research Fellowship grant NE/S01537X/1 (TJ)

FAPESP Young Researcher Grant # 2018/01847-0 (PG)

Czech University of Life Sciences Prague PhD scholarship FFWS CZU IGA number A_25_24 (PJ)

Author contributions:

Conceptualization: PB, AS, PJ, PG and LR

Methodology: PB, AS, PJ, LR, JLJ, MS, DB and LB

Formal analysis: PB, AS, PJ, RP, RM, LR and MS

Investigation: PB, AS, PJ, JLJ and MS

Writing – original draft: PB, AS, PJ and LR

Writing – review & editing: all authors

Competing interests: Authors declare that they have no competing interests.

Data and materials availability: The hydraulic traits dataset to replicate this is available on UKRI EIDC(*53*).The dendrometer growth rate data, the code used for data analysis and a summary table of the hydraulic traits data is available on DRYAD(*54*) . No new materials were created in this study.

Supplementary Materials

Materials and Methods

Figs. S1 to S9

Tables S1 to S6

References (55-99)

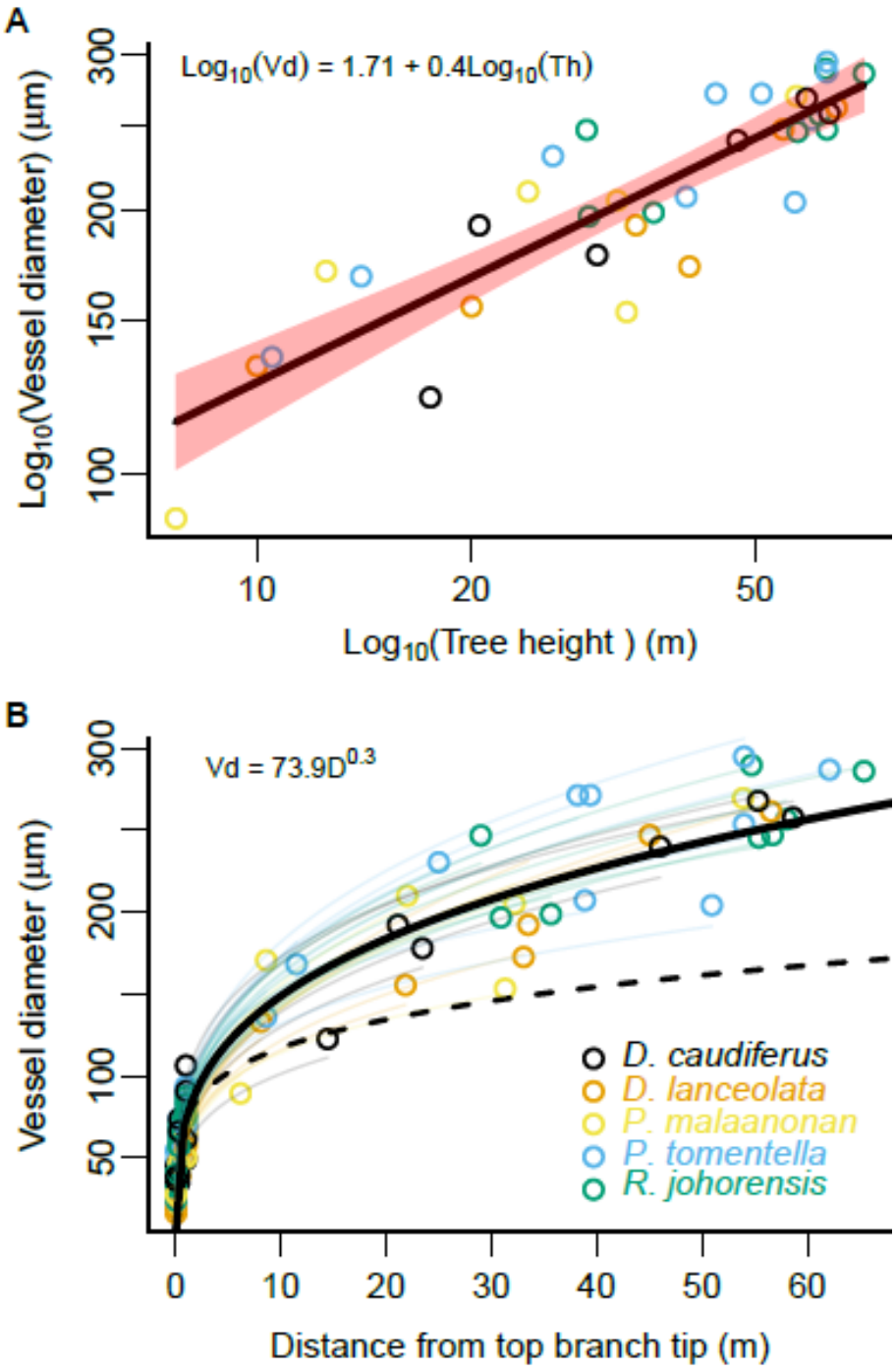

Fig. 1. Anatomical adjustments to compensate for increased path length with tree height. (**A**) vessel diameter at the base of the trunk as a function of tree height. (**B**) vessel diameter scaling with distance from the tip of upper branches. Solid lines are the model fit (all models are significant) and shaded area in (**A**) is the 95% confidence intervals for the fitted lines. Solid coloured lines in b) are the model fit to the individual. Solid line in (**B**) is the model from individual averaged coefficients. Dashed line in (**B**) is a fit forced to an exponent of 0.2. Different colours represent different species.

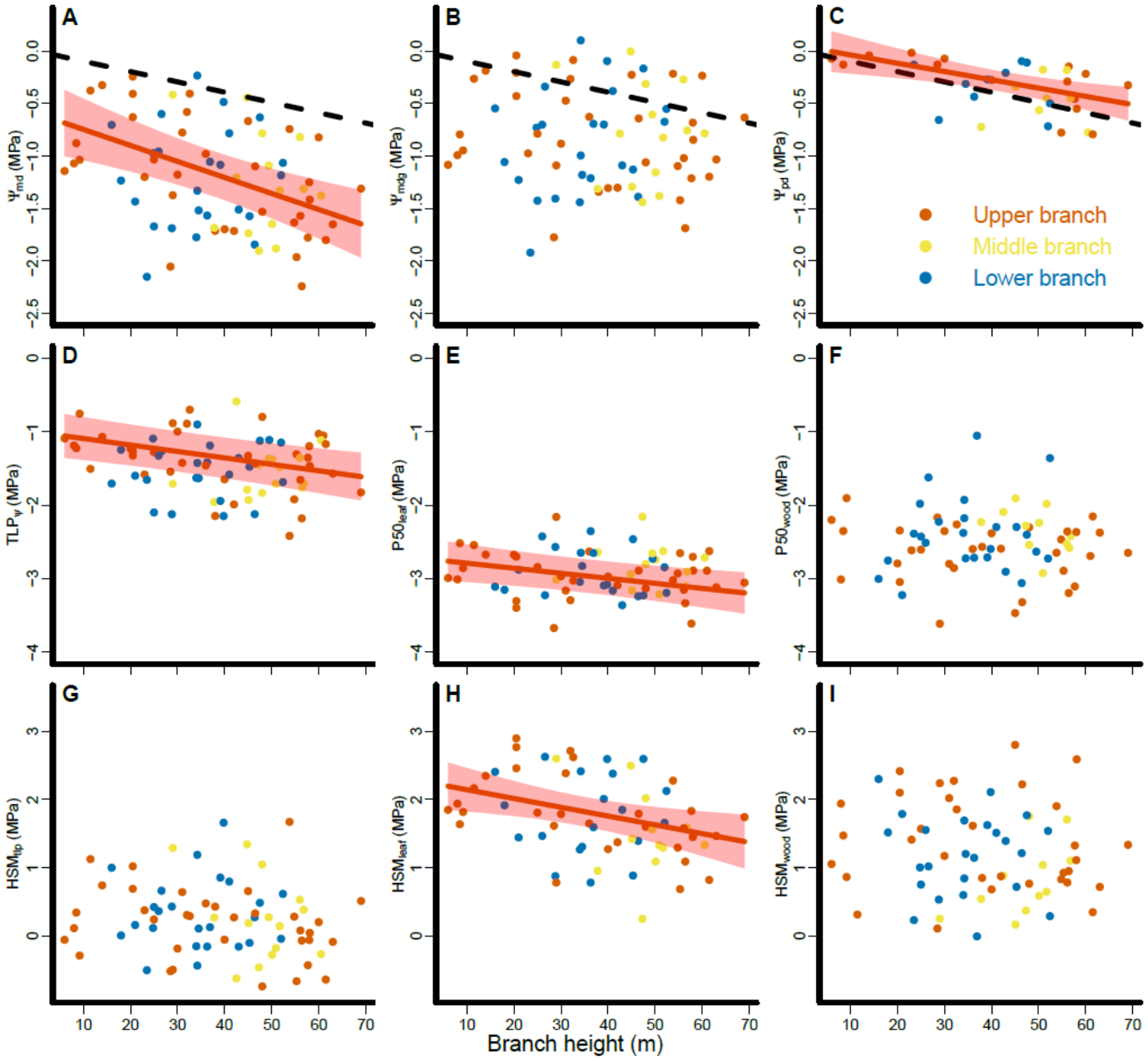

Figure 2. Changes in leaf water potential, key hydraulic thresholds and hydraulic safety margins with branch height. Colours indicate branches at different position within the tree crown of dipterocarp trees: upper crown branches (red), middle crown branches (yellow) and lower crown branches (blue). Panels **A-C** show water potential values, panels **D-F** show water potentials causing turgor loss and leaf and branch P_{50} and panels **G-I** show safety margins to turgor loss and leaf and branch P_{50}. Solid lines indicate the mixed effect model fit when significant (models are only significant for upper canopy branches), with the red polygon marking the 95% confidence interval. Model results are presented in Table 1. Dashed lines in **A-C** indicate the slope of the gravimetric water potential (i.e. -9.8 kPa m^{-1}, setting the theoretical maximum water potential any branch at that height should be able to maintain).

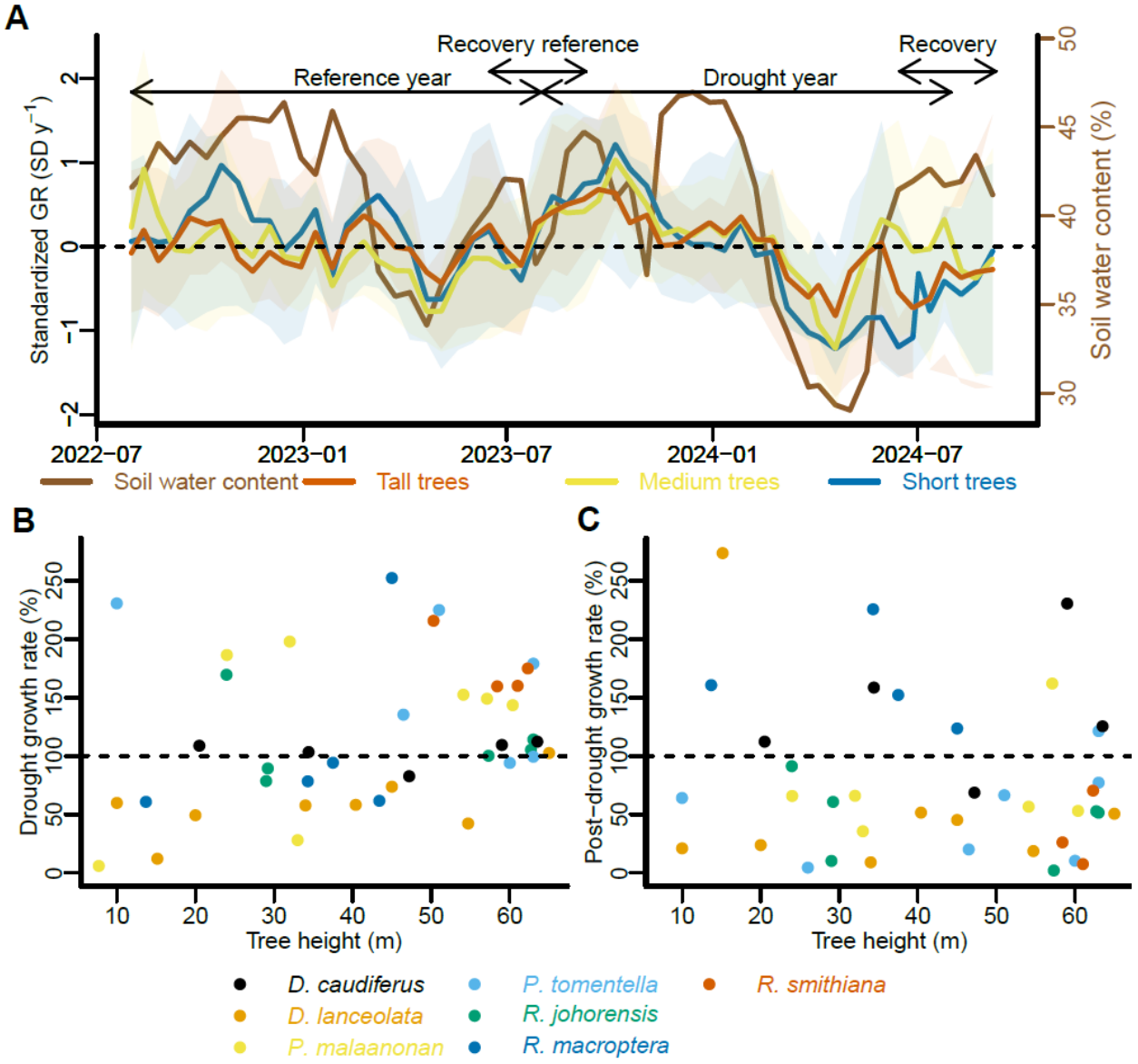

Figure 3. Tree height effect on dipterocarp trees growth during a strong ENSO-related drought. (**A**) Time series of standardized trunk growth rate (GR) for the 42 study trees and soil water content (brown line). Colours indicate tree sizes – red for tall trees (>50 m height), blue for short trees (<30 m height) and yellow for intermediate height trees (30 to 50 m). The shaded area in (**A**) marks ± 1SD band from the mean for each tree size category. Arrows indicate the regular year, drought year and recovery phase periods. The arrow labelled "recovery reference" is the same period in 2023 as the recovery period in 2024 and was used as the reference to evaluate the 2024 drought effect on the post-drought recovery. (**B-C**) Percentage change in tree diameter growth rate with tree height during the drought year relative to a regular year (**B**) and during the post-drought recovery phase in relation to the same period in the wet year (**C**). Horizontal line in **B-C** indicates 100% - trees above this value grew more during the drought year (**B**) or the recovery phase (**C**) than they grew during the regular year (**B**) or the same period the previous year (**C**).

Science
AAAS

Supplementary Materials for

Height does not impair the hydraulic system of the tallest tropical Dipterocarp trees

Paulo Bittencourt, Arne Scheire, Palasiah Jotan, Jehova Lourenço-Junior, Lindsay Banin, Mohd. Aminur Faiz bin Suis, David FRP. Burslem, Bradley Christoffersen, David Coomes, Peter Groenendijk, Steven Jansen, Tommaso Jucker, Radim Matula, Maurizio Mencuccini, Rafael Oliveira, Roman Plichta, Reuben Nilus, Rolando Robert, Martin Svátek, Lucy Rowland
Corresponding author: BittencourtP@cardiff.ac.uk

The PDF file includes:

Materials and Methods

This study was conducted in a Mixed Dipterocarp Forest in the Kabili Sepilok Forest Reserve, northeast Borneo (lat. 5°52'34" N, long. 117°56'58" E). The region has a mean monthly temperature of 26.5 ± 0.6°C (mean ± SD) and mean annual precipitation of 2640 ± 675 mm, with no regular dry period (<100 mm monthly rainfall). Intense supra-annual drought happens predictably associated to ENSO conditions (Fig. S7) (*36*, *55*). During those periods, intense drought-related mortality and growth reduction occurs in mixed dipterocarp forests (*56–61*). We collected plant material in three permanent alluvial forest plots of 4ha (*62*). Alluvial forests occur in lowland flat valleys, characterized by nutrient-rich and clayey soils (*36*, *62*) where dipterocarps trees >70 m height can occur (*63*). The plots are less than 1 km apart and so abiotic differences across them are negligible and they are very similar in terms of soil conditions, topography and mean elevation (*36*).

Plant material

We sampled 38 dipterocarp trees ranging from 7-71 m tall and diameter at breast height (1.3 m above ground or above buttress roots) from 9 to 153 cm from the five most abundant dipterocarp species with sufficient height variance across the plots (Fig. S1 and traits summary table on Dryad(*54*)): *Dipterocarpus caudiferus* Merr., *Dryobalanops lanceolata* Burck*, Rubroshorea johorensis* (Foxw.) P.S.Ashton & J.Heck*, Parashorea malaanonan* (Blanco) Merr. *and Parashorea tomentella* (Symington) Meijer. The sampling was conducted from April-June in 2022, during a year without any ENSO effects. The total aboveground biomass of the five species combined is 46.6% of the forest's biomass (Fig. S9). From each individual, we measured the diameter at breast height or above buttresses using a diameter tape and the tree height using a laser rangefinder (Forestry Pro II; Nikon, Tokyo, Japan), with height values confirmed by direct measurement from tree climbers. Branches were collected from an upper branch of each tree, as close to the top of the tree as could safely be collected and, in a fully sunlit location if the tree was not fully shaded. In addition, whenever the individuals had a sufficiently deep crown, from the lowest branch and from an intermediary branch, as close to the midpoint between the lowest and highest branch, as could safely be collected (Fig. S1). In each location, upper, middle and lower branching locations, four 1-2 m long branches were collected from the same location to allow sufficient material to be able to make all trait measurements. Two branches were used for xylem embolism resistance measurements, one branch for leaf embolism measurement and the last branch for measurements of leaf pressure-volume relations, wood anatomy and other traits (wood density, leaf-to-sapwood area ratio and leaf mass per area). The height of each branch was measured with the laser range finder, as was the distance back to the main trunk and to the ground from where the branch was cut, allowing us to estimate branch hydraulic pathlength. Using tree corers, we collected wood cores for anatomical analysis from the trunk at breast height, or above the buttress roots. Core collection height was also measured with a laser range finder. Immediately after collection, we stored the material in moist plastic bags and transported the collected material for analysis in laboratories in Sabah's Forest Research Centre, 10-30 minutes' walk from the plots. We installed a mini-weather station 3 m above a 65 m tree to monitor temperature and humidity (SHT3C, Sensirion), rainfall (ECRN-50, Meter) and active photosynthetic radiation (SQ500, Apogee) across the study period in the sites. A summary of symbols, definitions, units and measurements performed in each branch is presented in Table S1.

Tree water status

We measured the water potential of leaves of each of our study trees, at each branch sampling location (upper, middle, lower) using a pressure chamber (*64*) (Model 1515D; PMS, Albany, NY, USA). Water potential at midday (Ψ_{md} 11:30 – 13:00) and at midmorning (Ψ_{mm} 9:00-10:00) was measured on all trees. For a subset of 15 trees randomly selected from our dataset, we measured water potential at predawn (Ψ_{pd} 01:00 – 06:00). Due to dangers associated with climbing these trees in the dark, we could only sample one predawn water potential per day and only on trees within which it was safe to do so (total of 15 trees). We measured leaf water potential in the field within five minutes after leaf collection by the tree climbers. During the sampling, the climate was uniform and soils were well hydrated, allowing water potential measured across different days to be compared with limited bias. We used the measured values of Ψ to compute the gravity-compensated Ψ defined as the original Ψ in addition to the gravity effect caused by height at the sample location: 0.0098 MPa m^{-1} × sample height). We monitored the vapor pressure deficit (VPD) during water potential measurements using a temperature and humidity sensor (SHT3C, Laubisruetistrasse, Switzerland) inside a radiation shield placed 3m above the crown of a 65m tall dipterocarp. During midday measurements, VPD was 1.2 ± 0.5 kPa and during midmorning VPD was 0.7 ± 0.4 kPa.

Wood embolism resistance

We measured the embolism resistance of the collected branches using the automated pneumatic method for estimating xylem embolism (*30*, *65–67*). This method monitors xylem air content and Ψ of a dehydrating sample. We collected branches early in the morning, before mid-morning water potential measurements. After collection, we rehydrated 2 m long branches overnight to ensure curves started at full hydration status. The following day, we cut them into two 40-70 cm long samples, immediately connecting them to a M-Pneumatron (*66*). Bench dehydration (*68*) was used to induce embolism in the samples. The Ψ of dehydrating branches was measured with a pressure chamber throughout the dehydration period after the branch had been bagged for one hour to allow branch and leaf water potential to equilibrate. We stopped measuring the Ψ when values dropped below -8 MPa or when their leaves were hard, crispy and started dropping off, at which point we assume the branches were fully embolized. Full dehydration of the samples occurred within 2-4 days of starting the measurements, and full embolization of the branches was confirmed by verifying the existence of an air discharge plateau at low water potential values (*69*). From each vulnerability curve, we estimated the xylem water potential leading to 50% and 88% increase in xylem air content (P50 and P88), by fitting a sigmoidal equation to the curves (*70*). The P50 is considered a point of significant hydraulic damage and the P88 a point-of- no-return for tree death and thus trees are expected to strongly adjust hydraulic traits to prevent then crossing these thresholds (*71*). For each crown location in each tree, we used the average of the two measured samples as the final P50 and P88 values.

Leaf pressure-volume curves

We measured leaf turgor loss point, osmotic potential at saturation, bulk modulus of elasticity and water content at turgor loss point from pressure-volume curves, which relate leaf water content to leaf volume (*72*). After fully rehydrating branches, we monitored Ψ with a pressure chamber and leaf mass with an analytical scale during branch desiccation following a standardised method (*73*). Each leaf was then dried in an oven at 60^{o}C for at least 48h to obtain relative water content. We calculated the leaf water relations traits using the R package "pvldcurve" (*73*, *74*). For each branch, we measured two leaves and used the mean of the two leaves trait values for analysis.

Leaf embolism resistance

We measured leaf vulnerability to embolism using the optical method (*75*). We monitored leaf embolism on one leaf per branch in a 1-2 m long branch using a high-resolution transmission scanner (Epson Perfection V600), while Ψ was simultaneously monitored using a stem psychrometer (PSY1, ICT International, Australia). Branches were fully hydrated prior to the start of the measurements, and we monitored the leaves for at least 36 hours or until leaf water potential showed no further decline or until the leaves turned brown, at which point we assumed the leaf was fully embolized. We processed the images using ImageJ (*76*) (v1.54h) following a standard protocol (*77*) to calculate the percentage of embolism at the time the image was captured. We used these data and the Ψ from the psychrometer to calculate leaf embolism vulnerability curves from which we estimated leaf P50 and P88 (*70*).

Xylem anatomy

We measured vessel diameter distribution and vessel density at five, 33 and 100 cm distance from the tip on each of the branches sampled. Additionally, for each tree, we collected anatomical sample in the trunk at breast height or just above buttresses. All samples were inspected under a microscope to make sure they represented sapwood. Trunk samples were also collected from the outer 0.5-1 cm of the xylem and thus these samples are also unlikely to have contained any heartwood. We prepared cross-sections ranging from 15 µm to 35 µm in thickness using a sliding GSL1-microtome (*78*), samples were mounted on black double-sided adhesive tape and covered with a cover slip. We used a confocal laser scanning microscope (Leica SP8) to image the samples (*79*). We scanned several mosaics of images for each wood section and merged them using LAS X software (Leica, Germany) to form a single composite image per sample. We then measured xylem vessel distribution and density using ImageJ (*76*) (v1.54h) and GIMP (*80*) (v2.10.36) following standard vessel quantification guidelines (*81*). We note dipterocarps often present conductive imperforate tracheary elements in their xylem and we observed them in a pilot sample we analyzed using electron transmission microscopy. We could not differentiate them using confocal microscopy but they were much smaller than vessels and thus bellow the size threshold used in our analysis (10 micrometers).

We considered vessel diameter as the average of the maximum and minimum internal (lumen) diameter of vessels on each slide. We determined vessel density and vessel lumen fraction by summing the number of vessels and the area of vessel lumina within a given area, respectively (*82*). We calculated potential xylem hydraulic specific conductivity (K_{sp}) using the Hagen-Poiseuille law (*8*):

$$K_{sp} = (\pi \rho_w / 128\eta) \times N \times Dh^4$$

where ρ_w is the density of water (998.2 kg m^{-3}), η is the viscosity of water (1.002×10^{-3} Pa s) at 20 ºC, N is the vessel density (the number of vessels per mm^2 of xylem) and Dh is hydraulically weighted vessel diameter. Dh was calculated by exponentiating each vessel in a sample to the fourth, calculating the average and then taking the fourth root of this average. We calculated the sample xylem potential leaf-specific conductivity on branches by multiplying K_{sp} by sample xylem area to obtain xylem conductivity and then dividing it by the leaf area distal to the sampled location.

Wood and leaf traits and leaf-to-sapwood-area ratio

For each sample, we calculated wood density and wood saturated water content on all wood and trunk samples following Pérez-Harguindeguy et al. (2013) (*83*). We measured leaf area for each branch by scanning all leaves distal to the anatomy sampling location, 100 cm from the tip, using a scanner and calculated its total leaf area using ImageJ (*76*) and the LeafArea R package (*84*). We dehydrated the leaves at 60 ºC for 48h to measure their dry mass and calculate leaf mass per area. We calculated branch leaf-to-sapwood area ratio by dividing the total leaf area by the xylem cross-sectional area 100 cm from the tip.

Tree growth rate

We monitored trunk diameter growth rate for over 770 days (Fig. 3A) on 42 dipterocarp trees. Of these, 27 trees are the same trees for which we measured hydraulic traits in Bittencourt et al. (2022) (*36*), while including additional individuals from *Rubroshorea smithiana* (Symington) P.S.Ashton & J.Heck and *Rubroshorea. macroptera* (Dyer) P.S.Ashton & J.Heck (Table S5 and Table S6). We used point dendrometers (D1, TOMST, Czech Republic) (*85*, *86*) installed at breast height or above the buttresses to monitor micrometric changes in tree diameter. For large diameter trees, we installed two dendrometers in different radial positions of the trunk and used the average of the two sensors as a measure of diameter change of the tree trunk. We also monitored the soil water content of each plot at 0-15 cm depth in different locations using time domain reflectometry sensors (TMS-4, TOMST, Czech Republic) (*85*). We monitored the trees from August 2022 to March 2024, during which ENSO caused a period of drought, measured as unusually low soil moisture content lasting from March to August (Fig. 3A). Trunk diameter change was monitored every 30 minutes. We calculated daily growth rate as the change in maximum daily diameter between days and used a 14-day moving window to average each day's growth (*87*). With diametric growth rate we calculated basal area increment and used this to calculate relative growth rate as basal area increment divided by basal area. For each tree, we also calculated the percentage growth rate change from 2023, a slightly drier than average year, to the 2024 year, with a strong ENSO-driven drought. In addition, we calculated the change in growth during the recovery phase in 2024, after the drought ended (Fig. 3A) and compared this to the same period in 2023. For this, we divided the total growth rate of each tree during the ENSO year (August 2023 to August 2024) by the total growth rate in the year before (August 2022 to August 2023). Similarly, we divided the total growth rate in the recovery period (starting from when soil water content was fully recharged in July 2024 to October 2024) by the total growth rate for the same period in the previous year.

Climate data

We used the ERA5- Land (*88*) monthly averaged data from 1950-2025 (9 km resolution) to characterize the climate and to calculate the climatologic water deficit from 2023 to 2025 for the study region (Fig. S7). We calculated the climatic water deficit following the methods in Barros *et al.* 2019 (*42*), where it equals the monthly cumulative difference between evapotranspiration and precipitation across the time series, with all negative values set to zero (i.e., when precipitation was higher than evapotranspiration leading to saturated soil conditions).

Forest inventory, biomass and canopy height

To obtain the data which show the contribution of trees >70 meter to total forest biomass (Fig. S9B) and species maximum heights (Table S5) we obtained plot level height and diameter data. In the three 4-ha forest plots in the Kabili-Sepilok Forest Reserve where our sample trees are located, each tree ≥ 10 cm in diameter at breast height (DBH) (~840 trees per hectare), was identified. We used the DBH data measured in 2022 to calculate the total aboveground biomass using the BIOMASS package (*89*), with tree height estimated based on a local DBH-tree height allometry of 1572 trees measured in three mixed dipterocarp forests within Sabah (Kabili-Sepilok, Maliau and Danum Valley). The allometry data was fitted to a Weibull model (r2 = 0.80, RMSE = 5.47m). Tree wood density was retrieved from the BIOMASS package. For the 38 trees we studied, their biomass was estimated using the same biomass model, but with their own measured height, DBH and wood density. We used the same dataset as Jucker et al. (2018) (*63*) to generate a 1 m^2 resolution canopy height for our alluvial forests studied in Kabili-Sepilok Forest; obtained from aerial lidar scanning in 2014 (*90*).

Species maximum height

We estimated the maximum height of the five studied species by combining the data for the38 trees we sampled for hydraulic traits with data available in the Tallo database (*91*), totaling 419 measured individuals in multiple sites in Borneo (Fig. S9 C-H). For each species, we fitted a Weibull model to their allometry data. We estimated the maximum species height in three different ways: 1) as the 95th quantile of available tree height data, 2) as model predicted tree height for the maximum DBH observed for those species (165cm) and 3) as the maximum DBH observed across dipterocarps in the Tallo database (Fig. S9 and Table S5). All methods produced similar estimates and indicated the maximum species height for our species to be around 65m and that individuals with heights over 80 m are likely to be outliers, confirming our design captured the tallest individuals for those species.

Statistical analysis

We performed all analyses in the R statistical environment (v.4.2.2) (*92*). In mixed effect models, we tested the significance of the fixed effects using a log-likelihood test against the full model with one fixed effect removed at a time (*93*). For linear mixed effect models we used the NLME package (*94*, *95*), for the calculation of mixed model marginal and conditional pseudo-r2 values we used the MUMIN package (*96*). We calculated mixed model predictions 95% confidence intervals by generating predictions based on parametric bootstrapped models using the *bootMer* function of the lme4 package (*97*). We used the "lm" and "nls" functions from R's base package for fitting fixed effect linear models and non-linear models. For standardized major axis regression, we used the smatr package(*98*). We followed established best practices to diagnose the models, validate assumptions, test sensitivity to outliers, and assess robustness (*93*, *99*). For all statistical tests, a p-value of 0.05 was used as significance threshould.

Statistical analysis of vessel diameter adjustments with tree height and hydraulic pathway

To evaluate how vessel anatomy changes with tree height, we tested if the vessel diameters at the base of the trunk scaled with distance from the tip of the upper branch using a linear model with both axis $\log_{10}$ transformed (n = 37). We then evaluated the vessel diameter scaling with increasing hydraulic pathway. For each individual (n = 37 individuals, four samples per individual) we fitted log10 transformed vessel diameter to the log10 transformed distance from the tip using standardized major axis regression (*98*). The slope of the log-log relation equals the exponent and the log10 untransformed intercept equals the slope of the model vessel diameter ~ aDistance^{b}. We used the mean exponent of all individuals and its estimated confidence interval to evaluate if vessel diameter scales with distance from the branch tip with an exponent >0.2.

Statistical analysis of trait changes with branch height

To evaluate how traits change with branch height, we used linear mixed effect models. We used branch height as a fixed effect and species as a random effect on the hydraulic trait intercept. We analyzed data from upper, middle and lower crown branches separately to avoid confounding effects due to branch height and tree height being correlated and because not all trees had crowns deep enough for sampling lower and middle branches. For anatomical traits (K_{sp}, K_{sleaf}, vessel diameter and vessel density), we used the data measured at 1 m from the branch tip for this analysis. Sample numbers for each test are shown in Table S2 and S4.

Statistical analysis of within-tree trait changes with branch height

We tested if within-tree differences in hydraulic traits through the crown were related to tree height using mixed effect models. For each tree, we calculated the difference in hydraulic trait values between the upper and lower crown branches and related this value to the tree height as a fixed effect and species as random effect on the intercept. If tree height was not significant, we then tested whether upper crown branches had systematically different trait values to lower crown branches using a paired t-test. For anatomical traits (K_{sp}, K_{sleaf}, vessel diameter and vessel density), we used the data measured at 1 m from the branch tip for this analysis. Sample numbers for each test are shown in Table S3.

Statistical analysis of tree height effects on growth rates during drought conditions

We tested whether changes in trunk diameter growth rate during the ENSO-driven drought in 2023-2024 and in the recovery phase (when soil water content increased) were related to tree height using. For this we used mixed effect linear models with tree height as fixed effect and controlled for species differences by adding a random species effect on the intercept (n = 39 trees). We tested if relative growth rates were affected by soil water content (SWC) and tree height using a mixed effect model with a term for the interaction between tree height and SWC as variables (n = 2335). To control for repeated measures within each individual, we used the individual as a random factor affecting the intercept and as a random factor affecting the SWC slope. We also tested if our results were affected by

the two additional species not in the traits analysis (*R. smithiana* and *R. macroptera*) by repeating this analysis without these two species. As we found no relevant changes, we only present results for the full dataset analysis.

868

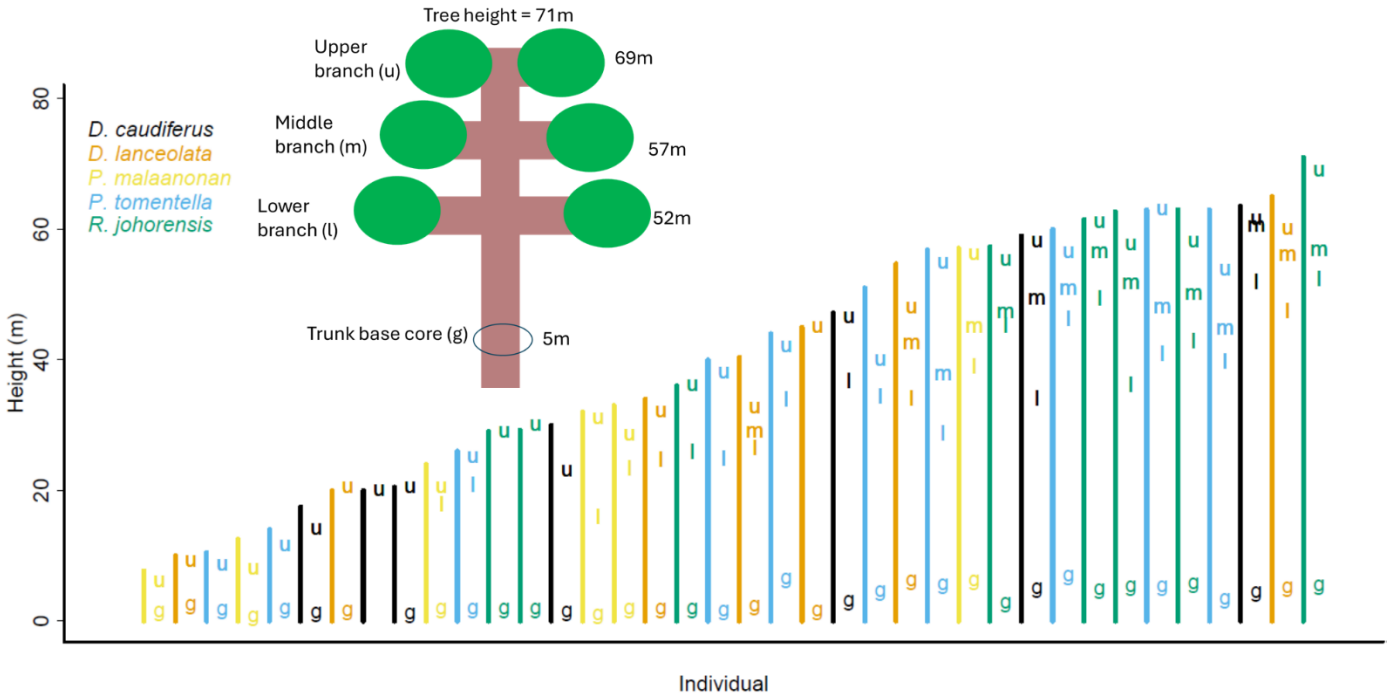

Figure S1. Tree height and sampling locations in each individual sampled tree. Each bar indicates one sampled tree. Colours indicate different species. Letters to the right of each bar indicate sampling location: trunk base, above buttress when present (g), lower crown branch (l), middle crown branch (m), upper crown branch (u). The tree sketch indicates where samples were taken for the tallest sampled individual.

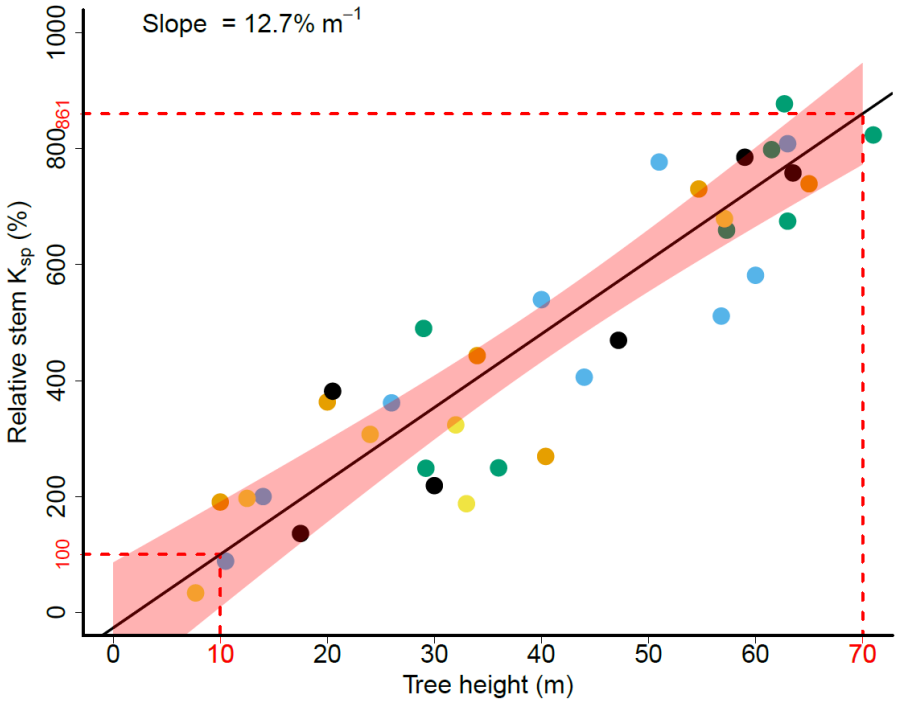

Figure S2. Trunk specific conductivity scaling with tree height. Potential xylem specific hydraulic conductivity (K_{sp}) at the base of the trunk as a function of tree height. Values shown are relative to predicted K_{sp} for a 10 m tall tree (i.e., a 10 m tall tree has 100% K_{sp}). Solid line is the model fit ($p < 0.001$) and shaded area is the 95% confidence interval for the fitted line. Different colours represent different species. Dashed lines highlight the relative K_{sp} for a 10 m tall tree (100%) and for a 70 m tall tree (861%, ~8.6 times that of a 10 m tall tree).

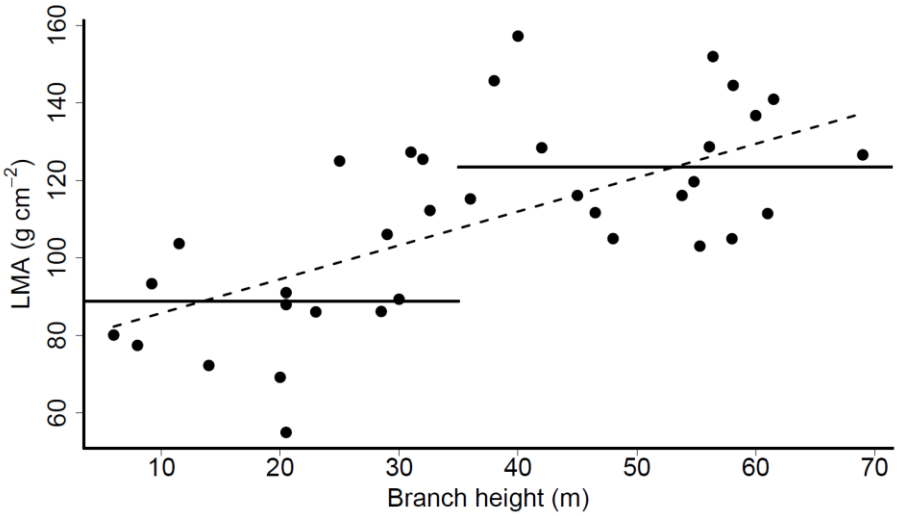

Figure S3. Relationship between leaf mass per area and branch height. Data shown is for upper crown branches. The dashed line indicates the model fit ($p = 0.01$; see Table S2). The solid lines indicate an alternative model where tree position - understory trees (<36 m height) and overstory trees – is tested as fixed effect instead of branch height affecting the leaf mass per area of branches. The alternative model with crown position as fixed effect is highly significant ($p < 0.001$) and has a lower AIC value than the branch height model (290.6 vs 302.4, respectively).

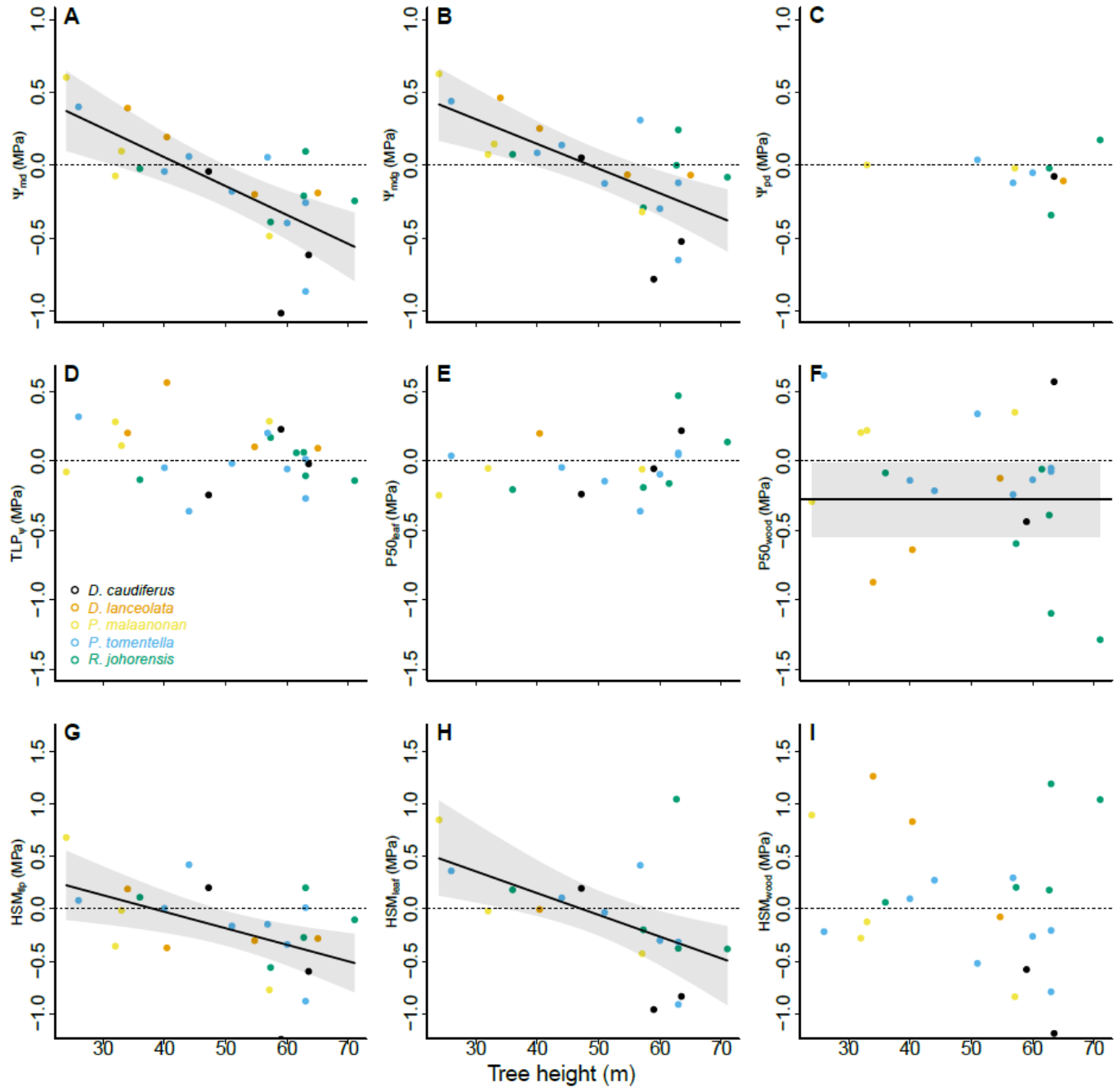

Figure S4. Within-tree changes (upper minus lower branch) in water potential, key hydraulic thresholds and hydraulic safety margins with tree height. Panels A-C show water potential values, panels D-F show water potentials causing turgor loss and leaf and branch P_{50} and panels G-I show safety margins to turgor loss and leaf and branch P_{50}. For each trait, the value shown is the difference between the trait value in the upper branch minus the trait value in the lower branch; the zero value thus represents the upper branch trait value and the dashed line marks this zero. Different colours represent different species (see species label on D). Bold solid lines indicate the model fit when significant with the polygon marking the 95% confidence

interval. Model results are presented in Table S3. The bold horizontal line in F indicates there is no relationship between that trait and tree height but that the difference between upper branches and lower branches is different from zero (paired t-test analysis).

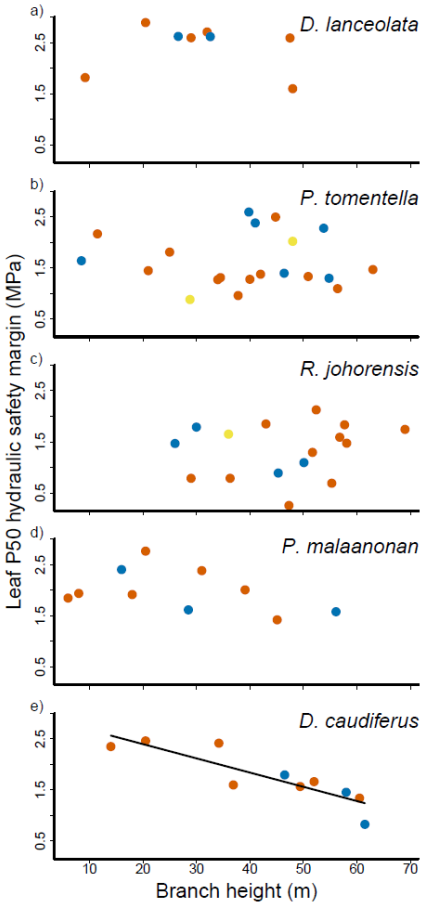

Figure S5. Relationship between leaf hydraulic safety margin (HSM_{leaf}) and branch height for each studied species. Data point colour indicates the sample branch position within a tree – upper crown branch (red), middle crown branch (yellow) and lower crown branch (blue). We note the significant relationship between HSM_{leaf} and branch height in Table S2 is driven by the *D. caudiferus* data only.

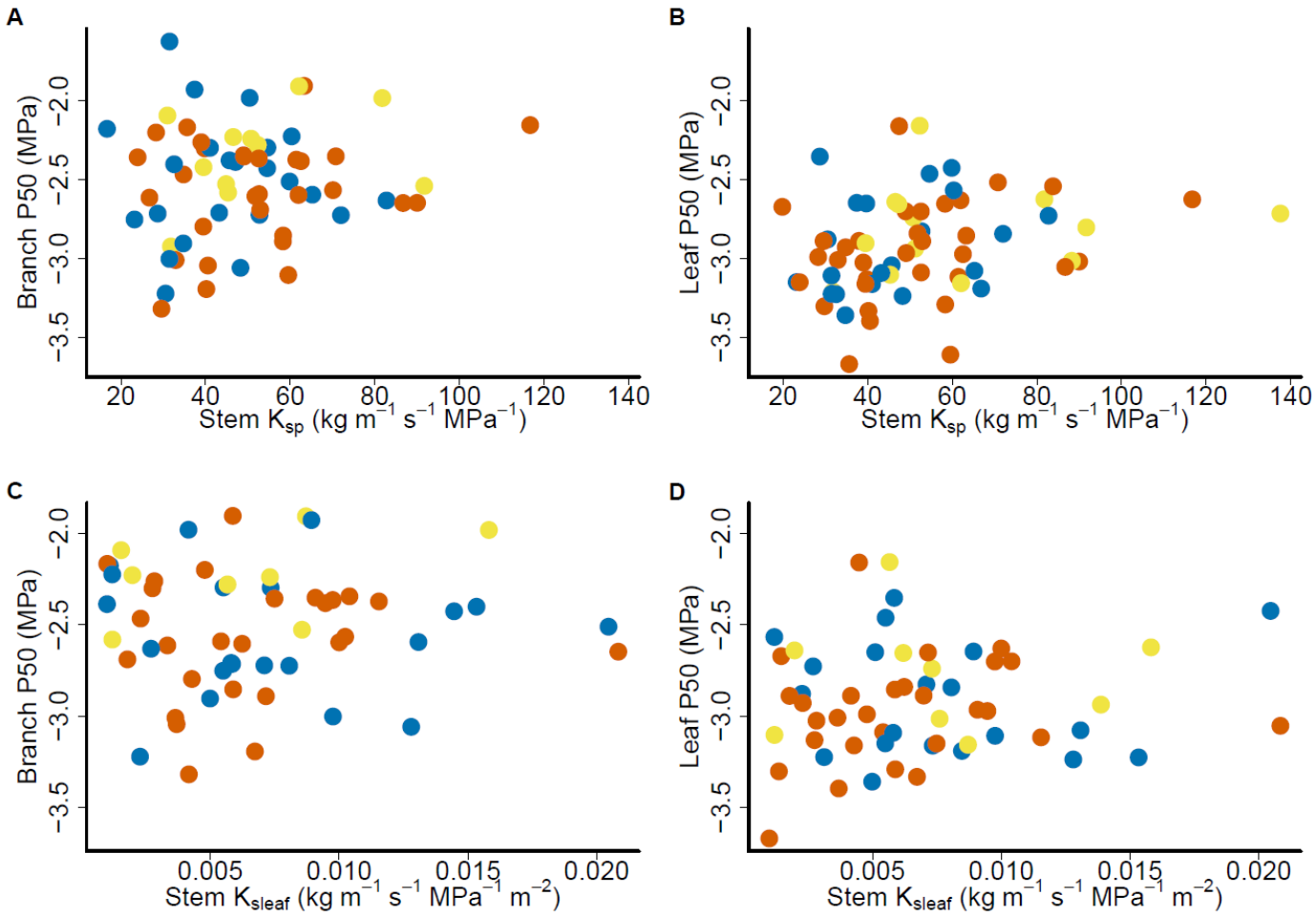

Figure S6. Hydraulic safety and efficiency relationship in dipterocarps. Relationship between embolism resistance and xylem specific conductivity, indicating an absence of a safety-efficiency trade-off in dipterocarps. Water potential leading to 50% loss of branch conductance (**A**) and leaf conductance (**B**) as a function potential xylem specific conductivity (K_{sp}; **A-B**) and xylem leaf specific conductivity (K_{sleaf}; **C-D**). Data point colour indicates the sample branch position within a tree – upper crown branch (red), middle crown branch (yellow) and lower crown branch (blue).

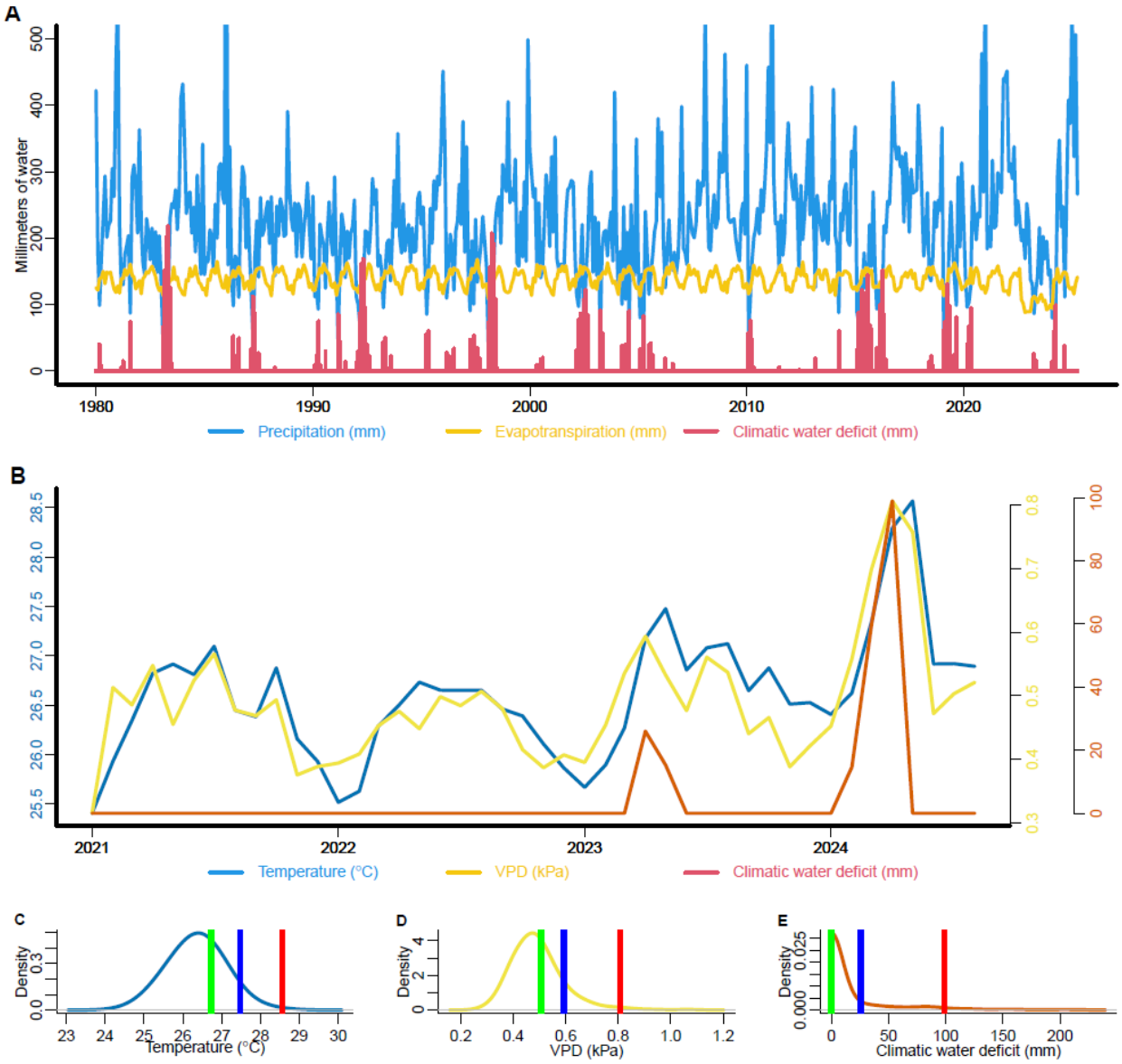

Figure S7. Meteorological conditions in the Sepilok mixed dipterocarp alluvial forest. (A) Time series of precipitation (blue line), evapotranspiration (orange line) and climatic water deficit (red vertical lines, also in mm) for the Sepilok region from 2003 to 2025. **(B)** Time series of temperature, vapor pressure deficit (VPD) and climatic water deficit in Sepilok from 2021 to September 2024. **(C-E)** Histograms of yearly maximum temperature (**C**), VPD (**D**) and climatic water deficit (**E**) from 1950 to 2025. Vertical bars in (**C-E**) mark the values for the year hydraulic traits data was collected (green) and the growth reference year (blue) and ENSO-related drought year (red) when growth data was also collected (see Fig. 3A).

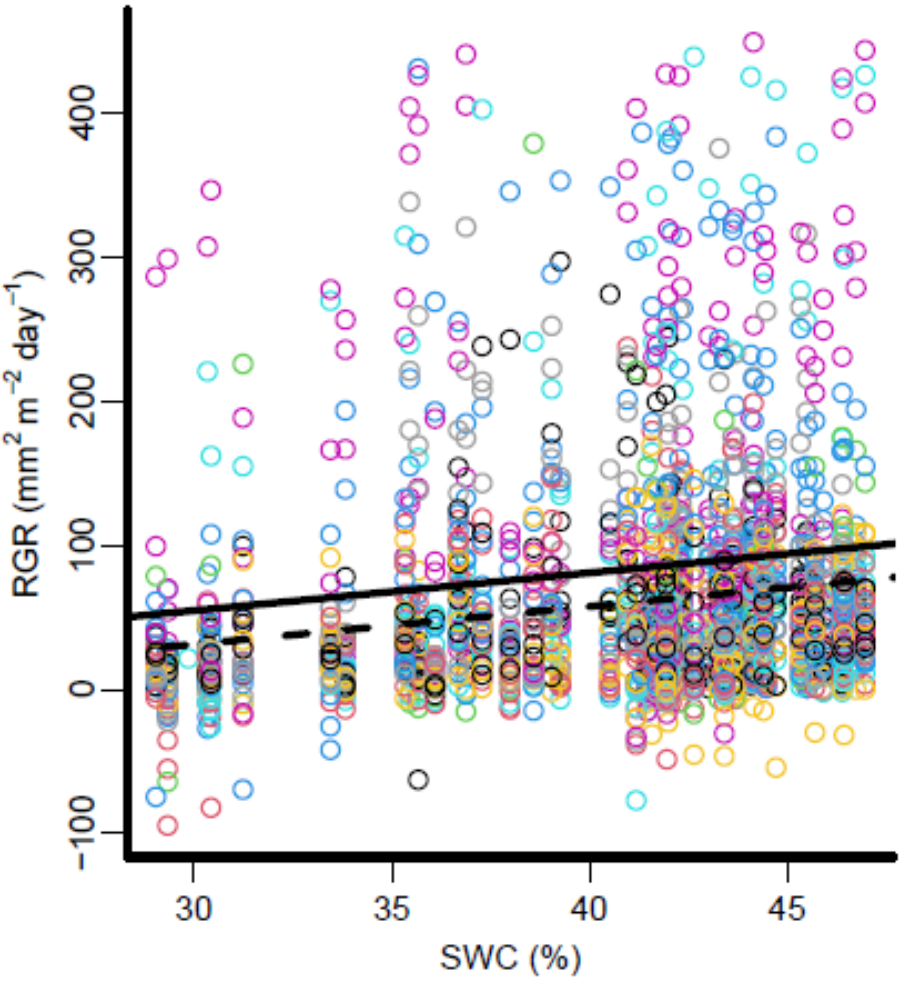

Figure S8. Dipterocarp growth rate sensitivity to soil water content. Data shows the effect of soil water content (SWC) on trunk relative growth rate (basal area increment divided by basal area; RGR). Each point is the average over a 14-day period. The black line indicates the fixed effect soil water content has on RGR from a model with each tree having a random intercept and random SWC slope. The SWC effect was independent of tree height. Tree height had an additive effect on RGR (i.e. not linked to soil water content). aThe lines show the model fit for a 30 m (continuous line) and 50 m (dashed line) tall tree, representing an average understory and overstory tree.

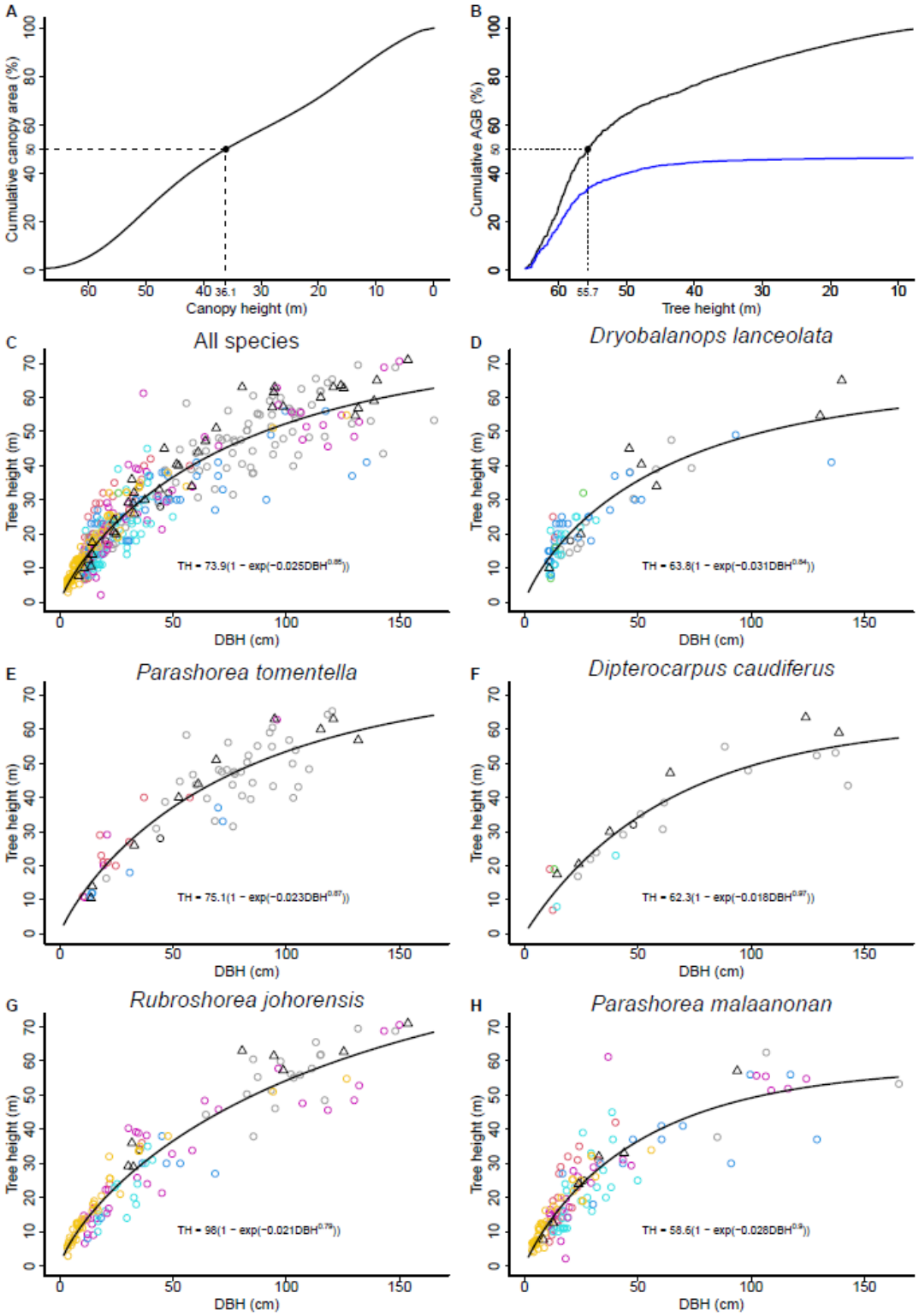

Fig. S9. Canopy height, above ground biomass and tree allometry in the Sepilok mixed dipterocarp alluvial forest. (A) Cumulative canopy area with decreasing canopy height based on aerial lidar scanning (~940 hectares). (**B**) Cumulative tree above ground biomass (AGB) with decreasing tree height (12 hectares of forest inventory) for all trees (black line) and for the 5 dipterocarp species used in this study (blue line). (**C-H**) Tree height and diameter at breast height (DBH) for the species studied combining data from the "Tallos" database (circles) with the trees measured in this study (triangle). (**C**) all species data combined. (**D-H**) individual species. The dashed lines and

941 circular point in a-b mark the canopy and tree height above which 50% of canopy area and above ground biomass
942 are contained. Different colours in **C-F** indicate data from different locations. The black line marks the Weibull
943 model fitted to the data.

Table S1. Traits measured in the branches of dipterocarp trees.

	Trait	Unit	Description
Water status	Ψ_{md}	MPa	Midday water potential
	Ψ_{mdg}	MPa	Gravity compensated water potential (Ψmd – 0.0098 Branch height)
	Ψ_{mm}	MPa	Midmorning (9-10h) water potential
	Ψ_{pd}	MPa	Predawn water potential
Leaf pressure-volume relations	TLP_{Ψ}	MPa	Turgor loss point
	OP	MPa	Cell osmotic potential at full turgor
	E	MPa	Bulk leaf modulus of elasticity
	TLP_{RWC}	unitless	Relative water content at TLP
Embolism resistance	$P50_{leaf}$	MPa	Water potential when branch or leaf loses 50% or 88% of its water transport capacity, as estimated from 50% increase in air extraction (branch) and 50% embolized area (leaf)
	$P88_{leaf}$	MPa	
	$P50_{wood}$	MPa	
	$P88_{wood}$	MPa	
Safety margins	HSM_{tlp}	MPa	Hydraulic safety margin, difference between Ψ_{md} and the point when the leaf loses turgor (HSM_{tlp}) or 50% water transport capacity (HSM_{leaf}) and when the branch xylem loses 50% water transport capacity (HSM_{wood})
	HSM_{leaf}	MPa	
	HSM_{wood}	MPa	
Anatomy and hydraulics	K_{sp}	$kg\ m^{-1}\ s^{-1}\ MPa^{-1}$	Potential xylem hydraulic specific conductivity
	K_{sleaf}	$kg\ m^{-2}\ s^{-1}\ MPa^{-1}$	Potential leaf specific hydraulic conductivity
	Vessel diameter	µm	Mean xylem vessel diameter
	Vessel density	mm^{-2}	Number of xylem vessels per unit area
	LA:SA	$m^2\ cm^{-2}$	Leaf-to-sapwood area ratio
Leaf traits	Leaf size	cm^2	Area of the leaf
	Leaf thickness	mm	Thickness of leaf lamina
	LMA	$g\ m^{-2}$	Leaf mass per area
Wood traits	WD	$g\ cm^{-3}$	Branch wood density
	Wood SWC	$g\ cm^{-3}$	Branch wood saturated water content

Table S2. Effect of branch height on upper crown branch hydraulic traits of our study trees. Results are from mixed models with branch height as fixed effect and species as a random effect on the intercept of the trait (see also Fig. 2). See Table S1 for details on traits and acronyms.
"Species σ^2" is the variance of the random species effect. Values for fixed terms intercept and slope are presented as estimate ± standard error. R^2m is the marginal coefficient of determination and R^2c is the conditional coefficient of determination. Ψ_{md}, Ψ_{mdg}, Ψ_{mm} and Ψ_{pd} are the leaf water potential at midday, at midday compensated by gravity, at midmorning and at predawn.
*Leaf mass per area (LMA) did not change with height when only non-understory trees (>36 m height) are considered, although understory trees have a lower LMA than canopy and emergent trees. See Fig. S3 for details.

	Trait	Intercept	Branch height	Species σ^2	R^2m	R^2c	p	n
Water status	Ψ_{md}	-0.59 ± 0.19	-0.015 ± 0.004	0.04	0.27	0.40	<0.001	36
	Ψ_{mdg}	-0.80 ± 0.11					0.18	36
	Ψ_{mm}	-0.41 ± 0.19	-0.010 ± 0.004	0.03	0.15	0.25	0.016	35
	Ψ_{pd}	0.04 ± 0.11	-0.009 ± 0.002	0.00	0.43	0.43	0.010	15
Leaf pressure-volume relations	TLP_{Ψ}	-1.00 ± 0.17	-0.009 ± 0.002	0.09	0.15	0.66	<0.001	37
	OP	-0.88 ± 0.15	-0.007 ± 0.002	0.07	0.11	0.63	0.005	37
	E	-1.55 ± 0.14					0.40	37
	TLP_{RWC}	91.7 ± 0.91					0.10	37
Embolism resistance	$P50_{leaf}$	-2.72 ± 0.15	-0.007 ± 0.002	0.06	0.13	0.55	0.010	34
	$P88_{leaf}$	-3.35 ± 0.11					0.43	33
	$P50_{wood}$	-2.64 ± 0.07					0.50	33
	$P88_{wood}$	-3.48 ± 0.18					0.72	33
Safety margins	HSM_{tlp}	0.41 ± 0.12					0.22	35
	HSM_{leaf}	2.21 ± 0.21	-0.01 ± 0.005	0.05	0.12	0.28	0.044	31
	HSM_{wood}	1.40 ± 0.14					0.46	33
Anatomy and hydraulics	K_{sp}	46.7 ± 5.7					0.82	35
	K_{sleaf}	0.006 ± 0.001					0.14	30
	Vessel diameter	72.0 ± 5.5					0.24	34
	Vessel density	47.8 ± 6.6					0.25	36
	LA:SA	0.55 ± 0.08					0.42	36
Leaf traits	Leaf size	77.6 ± 9.6	-0.74 ± 0.14	329.6	0.26	0.72	<0.001	36
	Leaf thickness	0.17 ± 0.02	0.001 ± 0.001	0.001	0.18	0.77	<0.001	37
	LMA*	77.0 ± 8.1	0.87 ± 0.16	108.7	0.40	0.58	<0.001	35
Wood traits	WD	0.45 ± 0.03	0.002 ± 0.001	0.002	0.16	0.58	0.003	36
	Wood SWC	0.53 ± 0.01					0.77	36

Table S3. **Effect of tree height on within-tree changes in hydraulic traits of our study trees.** For each tree, the difference between trait value at the upper branch minus trait value at the lower branch was calculated (see also Fig. S3). See Table S1 for details on traits and acronyms. We first tested if this difference was related to tree height using a mixed model with tree height as fixed effect and species as a random effect on the intercept. If tree height is not a significant effect, we test if the upper to lower trait difference is significantly different from 0 using a paired t-test (p-values labelled with * when significant). Species $\sigma^{2"}$ is the variance of the random species effect. Values for fixed terms intercept and slope are presented as estimate ± standard error. For paired t-test analysis, intercept values are the mean difference ± confidence interval. R^2m is the marginal coefficient of determination and R^2c is the conditional coefficient of determination.

	Trait	Intercept	Tree height slope	Species σ^2	R^2m	R^2c	P	n
Water status	Ψ_{md}	0.85 ± 0.22	-0.02 ± 0.01	0.01	0.49	0.58	<0.001	24
	Ψ_{mdg}	0.82 ± 0.21	-0.017 ± 0.004	0.01	0.43	0.53	<0.001	18
	Ψ_{mm}	-0.22 ± 0.09					0.006*	22
	Ψ_{pd}	-0.05 ± 0.04					0.86	10
Leaf pressure-volume relations	TLP_{Ψ}	0.06 ± 0.05					0.36	25
	OP	0.06 ± 0.05					0.18	25
	E	0.07 ± 0.12					0.60	25
	TLP_{RWC}	0.45 ± 0.64					0.49	25
Embolism resistance	$P50_{leaf}$	-0.04 ± 0.04					0.21	14
	$P88_{leaf}$	-0.17 ± 0.11					0.92	20
	$P50_{wood}$	-0.34 ± 0.16					0.02*	24
	$P88_{wood}$	-0.75 ± 0.38					0.01*	21
Safety margins	HSM_{tlp}	0.60 ± 0.29	-0.016 ± 0.006	0.01	0.25	0.25	0.012	24
	HSM_{leaf}	0.98 ± 0.42	-0.021 ± 0.008	0.01	0.27	0.28	0.021	19
	HSM_{wood}	0.17 ± 0.18					0.25	23
Anatomy and hydraulics	K_{sp}	7.1 ± 3.5					0.90	25
	K_{sleaf}	0.001 ± 0.001					0.13	22
	Vessel diameter	3.4 ± 3.1					0.24	25
	Vessel density	-7.6 ± 4.6					0.57	25
	LA:SA	-0.05 ± 0.06					0.80	22
Leaf traits	Leaf size	-3.7 ± 3.6					0.80	23
	Leaf thickness	0.006 ± 0.006					0.77	25
	LMA	8.7 ± 4.9					0.46	21
Wood traits	WD	0.002 ± 0.02					0.32	24
	Wood SWC	0.02 ± 0.01					0.25	22

Table S4. Effect of branch height on lower and middle crown branch hydraulic traits of our study trees. Results are from mixed models with branch height as fixed effect and species as a random effect on the intercept of the trait. See Table S1 for details on traits and acronyms.
Values for intercept are presented as estimate ± standard error. The branch height effect was not significant for any of the models and thus its coefficient is omitted. The p-value and sampling number for the significance of the branch height effect are presented in the columns "p" and "n", respectively.

		Lower branch			Middle branch		
	Trait	Intecept	p	n	Intecept	p	n
Water status	Ψ_{md}	-1.26 ± 0.14	0.85	24	-1.19 ± 0.11	0.37	14
	Ψ_{mdg}	-0.85 x 0.12	0.26	24	-0.79 x 0.14	0.71	14
	Ψ_{mm}	-0.58 x 0.12	0.09	19	-0.88 x 0,14	0.12	14
	Ψ_{pd}	-0.34 x 0.07	0.73	10	-0.46 x 0.08	0.10	8
pressure-volume relations	TLP_{Ψ}	-1.46 x 0.14	0.53	25	-1.54 x 0.14	0.41	15
	OP	-1.24 x 0.11	0.58	25	-1.26 x 0.08	0.18	15
	E	-1.58 x 0.14	0.72	24	-1.35 x 0.20	0.08	15
	TLP_{RWC}	91.3 x 1.45	0.48	25	88.4 x 2.35	0.36	15
Embolism resistance	$P50_{leaf}$	-2.93 x 0.09	0.12	21	-2.82 x 0.08	0.92	13
	$P88_{leaf}$	-3.23 x 0.08	0.60	21	-2.98 x 0.09	0.80	13
	$P50_{wood}$	-2.34 x 0.13	0.52	25	-2.28 x 0.08	0.058	10
	$P88_{wood}$	-2.92 x 0.29	0.84	21	-2.77 x 0.42	0.40	10
Safety margins	HSM_{tlp}	0.33 x 0.11	0.87	24	0.27 x 0.17	0.21	14
	HSM_{leaf}	1.86 x 0.19	0.70	20	1.53 x 0.22	0.28	12
	HSM_{wood}	1.18 x 0.12	0.63	24	0.92 x 0.26	0.08	9
Anatomy and hydraulics	K_{sp}	44.0 x 3.6	0.077	24	60.1 x 7.36	0.75	15
	K_{sleaf}	0.007 x 0.001	0.57	24	0.007 x 0.001	0.75	11
	Vessel diameter	69.7 x 4.9	0.22	25	75.5 x 4.0	0.65	15
	Vessel density	51.1 x 9.0	0.84	25	41.2 x 6.6	0.96	15
	LA:SA	0.45 x 0.07	0.65	22	0.67 x 0.16	0.83	11
Leaf traits	Leaf size	43.4 x 7.7	0.18	23	40.9 x 6.6	0.31	11
	Leaf thickness	0.22 x 0.02	0.49	25	0.23 x 0.02	0.58	14
	LMA	126.7 x 12.7	0.55	24	111.7 x 30.5	0.83	11
Wood traits	WD	0.51 x 0.02	0.8	25	0.52 x 002	0.92	14
	Wood SWC	0.50 x 0.01	0.26	22	0.52 x 0.02	0.33	13

Table S5. Structure and size of the studied species. Tree height, diameter at breast height, number of trees sampled per species (n), their contribution to forest aboveground biomass (AGB) and the estimated species maximum height. Species maximum height was estimated from a dataset combining species data from the tree allometry database "Tallo" and the data from individuals in our study (see Fig. S9 and Methods). Species maximum height was estimated from the 95th quantile of the tree height distribution (95th Q) and from Weibull allometric models for each species for two different stem diameters at breast height – 165 cm, the maximum observed within those species and 210 cm, the maximum observed for all dipterocarps in Tallo (Model 165 cm and Model 210 cm columns). Model RMSE is the root mean squared error of tree height estimation for each species' model.

					Maximum species height (m)			
Species	Height range (m)	DBH range (m)	n	AGB (%)	95th Q	Model 165cm	Model 210cm	Model RMSE
Dipterocarpus caudiferus	17.5 - 63.5	14 - 139	7	5.2	46.3	56.8	59.5	4.8
Dryobalanops lanceolata	10 - 65	11 - 140	7	3.5	62.9	64.1	68.0	6.7
Parashorea malaanonan	7.7 - 57.1	8 - 94	6	2.9	63.0	68.4	75.0	5.7
Parashorea tomentella	10.5 - 63	14 - 132	10	17.6	54.9	55.3	57.0	6.2
Rubroshorea johorensis	29 - 71	30 - 154	8	17.2	58.3	57.4	59.8	5.4

Table S6. Description of trees monitored for growth rate. Species, tree height and total number of dipterocarp trees which we monitored their diametric growth rates with high-resolution dendrometers.

Species	Tree height range (m)	Total trees
Dipterocarpus caudiferus	20 - 63.5	6
Dryobalanops lanceolata	10 - 65	7
Parashorea malaanonan	7.7 - 57.1	5
Parashorea tomentella	10.5 - 63	6
Rubroshorea johorensis	29 - 63	6
Rubroshorea macroptera	13.7 - 45	5
Rubroshorea smithiana	41.8 - 65	5